Bioorganic Chemistry 91 (2019) 103097

Contents lists available at ScienceDirect

Bioorganic Chemistry

journal homepage: www.elsevier.com/locate/bioorg

Synthesis, molecular docking, and biological evaluation of 3-oxo-2-tolylhydrazinylidene-4,4,4-trifluorobutanoates bearing higher and natural alcohol moieties as new selective carboxylesterase inhibitors

Galina F. Makhaeva[a], Natalia A. Elkina[b], Evgeny V. Shchegolkov[b], Natalia P. Boltneva[a], Sofya V. Lushchekina[c], Olga G. Serebryakova[a], Elena V. Rudakova[a], Nadezhda V. Kovaleva[a], Eugene V. Radchenko[d], Vladimir A. Palyulin[d], Yanina V. Burgart[b], Victor I. Saloutin[b], Sergey O. Bachurin[a], Rudy J. Richardson[e,f,*]

[a] Institute of Physiologically Active Compounds Russian Academy of Sciences, Chernogolovka 142432, Russia
[b] Postovsky Institute of Organic Synthesis, Urals Branch of Russian Academy of Sciences, Yekaterinburg 620990, Russia
[c] Emanuel Institute of Biochemical Physics Russian Academy of Sciences, Moscow 119334, Russia
[d] Department of Chemistry, Lomonosov Moscow State University, Moscow 119991, Russia
[e] Departments of Environmental Health Sciences and Neurology, University of Michigan, Ann Arbor, MI 48109, USA
[f] Center for Computational Medicine and Bioinformatics, University of Michigan, Ann Arbor, MI 48109, USA

ARTICLE INFO

Keywords:
3-oxo-2-tolylhydrazinylidene-4,4,4-trifluorobutanoates
Higher alcohols
Natural alcohols
Transesterification
Esterase profile
Carboxylesterase
Inhibitors
Molecular docking
Antioxidant activity
ABTS assay

ABSTRACT

To search for effective and selective inhibitors of carboxylesterase (CES), a series of 3-oxo-2-tolylhydrazinylidene-4,4,4-trifluorobutanoates bearing higher or natural alcohol moieties was synthesized via pre-transesterification of ethyl trifluoroacetylacetate with alcohols to isolate transesterificated oxoesters as lithium salts, which were then subjected to azo coupling with tolyldiazonium chloride. Inhibitory activity against porcine liver CES, along with two structurally related serine hydrolases, acetylcholinesterase and butyrylcholinesterase, were investigated using enzyme kinetics and molecular docking. Kinetics studies demonstrated that the tested keto-esters are reversible and selective mixed-type CES inhibitors. Analysis of X-ray crystallographic data together with our IR and NMR spectra and QM calculations indicated that the *Z*-isomers were the most stable. The kinetic data were well explained by the molecular docking results of the *Z*-isomers, which showed specific binding of the compounds in the CES catalytic active site with carbonyl oxygen atoms in the oxyanion hole and non-specific binding outside it. Some compounds were studied as inhibitors of the main human isozymes involved in biotransformation of ester-containing drugs, hCES1 and hCES2. Esters of geraniol (**3d**) and adamantol (**3e**) proved to be highly active and selective inhibitors of hCES2, inhibiting the enzyme in the nanomolar range, whereas esters of borneol (**3f**) and isoborneol (**3g**) were more active and selective against hCES1. Computational ADMET studies revealed that all test compounds had excellent intestinal absorption, medium blood-brain barrier permeability, and low hERG liability risks. Moreover, all test compounds possessed radical-scavenging properties and low acute toxicity. Overall, the results indicate that members of this novel series of esters have the potential to be good candidates as hCES1 or hCES2 inhibitors for biomedicinal applications.

1. Introduction

Mammalian carboxylesterases (CES, EC 3.1.1.1) are serine esterases that belong to the α,β-hydrolase protein superfamily. They have broad substrate specificity and catalyze the hydrolysis of compounds containing ester, thioester, and amide bonds [1]. Although CESs are mainly associated with Phase I biotransformation of drugs and environmental toxicants [2–5], they can also hydrolyze endogenous esters and thioesters, and some of these enzymes play important physiological roles in lipid metabolism and energy homeostasis [6–8].

The primary CES enzymes in humans (hCES) include hCES1 and hCES2. These two isozymes share 47% protein sequence identity, but

* Corresponding author at: Molecular Simulations Laboratory, M6065 SPH-II 2029, University of Michigan, 1415 Washington Heights, Ann Arbor, MI 48109-2029, USA.
E-mail address: rjrich@umich.edu (R.J. Richardson).

https://doi.org/10.1016/j.bioorg.2019.103097
Received 8 May 2019; Received in revised form 25 June 2019; Accepted 28 June 2019
Available online 03 July 2019

they exhibit differential tissue distribution as well as distinct substrate and inhibitor specificities [1,5]. hCES1 expression is highest in liver, whereas hCES2 expression is highest in intestine [4,5,9,10]. hCES1 prefers ester substrates derived from bulky acyl groups and small alcohol groups: e.g., clopidogrel, cocaine, enalapril, imidapril, oseltamivir and meperidine. In contrast, hCES2 prefers ester substrates with small acyl groups and large alcohol groups: e.g., irinotecan, capecitabine, flutamide and procaine [10,11].

Given the scope of their activities in the biotransformation of exogenous and endogenous compounds, there has been considerable interest in the discovery of potent and selective inhibitors of hCES1 and hCES2 to modulate the pharmacokinetics of endobiotics and CES-substrate drugs in medically beneficial ways [10,12–14].

Compounds with a 1,2-dione scaffold have been identified as the most important chemical structures for CES inhibition. For example, aryl-1,2-diones (benzil and its analogues), alkyl-1,2-diones, isatins, and 1,2-quinones have been found to exert potent and selective inhibitory effects toward hCES1 or hCES2, yet they do not exhibit untoward inhibitory effects on human acetylcholinesterase (AChE) or butyrylcholinesterase (BChE) [11,14].

Selective CES inhibitors with low acute toxicity have been found among carbamates. These are O-carbamoylated 1-hexafluoroisopropanols, found by our group [15], and carbamates WWL113 and WWL229, selectively inhibiting mouse CES3, which is a hCES1 orthologue found by Cravatt's group [16].

In recent years, searching for specific and potent CES inhibitors from phytochemicals has attracted increasing attention [17,18]. Different classes of natural compounds such as tanshinones, β-lapachones containing a 1,2-dione moiety, flavonoids, and triterpenoids have been found with potent inhibitory effects against hCESs [11].

Tanshinones, phenanthrene-quinone derivatives isolated from the Chinese herb Danshen [19], are potent inhibitors of both hCES1 and hCES2, but they exhibit poor selectivity and specificity toward CES1 [20]. β-Lapachone, with a *cis*-coplanar 1,2-dione moiety, is a potent and reversible CES inhibitor that has greater specificity toward hCES2 than hCES1 [21]. Flavonoids are polyphenolic products widely distributed in fruits and vegetables [22,23], and recent studies have demonstrated that some of these compounds (e.g., bavachinin, coryfolin, and corylin) potently inhibit both hCES1 and hCES2 [24,25]. Triterpenoids are a diverse group of natural products with wide distribution, high chemical diversity, and important pharmacological properties [26,27]. A series of natural triterpenoids was tested for their inhibitory effects against carboxylesterases CES1 and CES2. Two pentacyclic triterpenoids, including oleanolic acid and ursolic acid, displayed strong inhibitory effects on CES1 [28].

We have previously shown that ethyl (methyl) 2-arylhydrazinylidene-3-oxo-3-polyfluoroalkylpropionates and their cyclic analogues, 7-hydroxy-7-polyfluoroalkyl-4,7-dihydroazolo[5,1-c][1,2,4]triazines, are potent and selective inhibitors of porcine liver CES that afford rich opportunities for structural modification [29–33]. In accord with the increased interest in plant-derived compounds and their synthetically modified derivatives as inhibitors of hCES1 and hCES2, a promising avenue of directed functionalization of 2-arylhydrazinylidene-3-oxoesters to create efficient and selective inhibitors of CES is the introduction of higher or natural alcohol moieties into the structure of 2-arylhydrazinylidene-3-oxo-3-polyfluoroalkylpropionates.

Here, we report the synthesis of trifluoromethyl-containing 2-tolylhydrazinylidene-3-oxoesters bearing various natural or higher alcohol moieties **3a-j**. We performed a biological evaluation of the compounds as inhibitors of porcine liver CES along with human erythrocyte acetylcholinesterase (EC 3.1.1.7, AChE) and equine serum butyrylcholinesterase (EC 3.1.1.8, BChE). In addition, we studied some of the compounds as inhibitors of human hCES1 and hCES2. To gain insight into the structural aspects of CES inhibition, we carried out molecular docking of the compounds to the active site of human CES1 and a homology models of human CES2 and porcine CES. To assess potential pharmacokinetic properties of the new structures, we determined ADMET profiles computationally. Finally, taking into account the close proximity of CES and cytochrome P-450 as enzymes of Phase I metabolism of xenobiotics [34,35], we assessed the antiradical activity of the compounds by the ABTS assay, as their potential hepatoprotective effect, and also we determined the acute toxicity of the compounds in mice.

2. Experimental section

2.1. Chemistry

All solvents, chemicals, and reagents were obtained commercially and used without purification. Melting points were measured in open capillaries on a Stuart SMP30 melting point apparatus and uncorrected. The IR spectra were recorded on a Thermo-Nicolet 6700 FT-IR spectrometer at 4000–400 cm^{-1} using the frustrated total internal reflection (FTIR) method. The ^{1}H (^{13}C) NMR spectra were registered on a Bruker Avance 500 spectrometer, 500 MHz (125 MHz) relative to $SiMe_4$. The ^{19}F NMR spectra were obtained on a Bruker Avance 500 spectrometer (470 MHz) using C_6F_6 as an internal standard. The chemical shifts were converted from C_6F_6 to CCl_3F. The microanalyses (C, H, N) were carried out on a Perkin Elmer PE 2400 series II elemental analyzer.

2.2. Crystal structures

A single crystal of compound **3f** was obtained by crystallization from acetonitrile. The X-ray studies were performed on an Xcalibur 3 CCD diffractometer with a graphite monochromator, φ/ω scanning, λMoK_α 0.71073 Å radiation, at T 295(2) K. The registration of absorption was carried out analytically by the model of a multi-faceted crystal using the program CrysAlis RED 1.171.29.9. Main crystallographic data for **3f**: $C_{21}H_{25}F_3N_2O_3$, M = 410.43, space group $P3_2$, trigonal, a = 23.8333(12), b = 23.8333(12), c = 12.8114(7) Å, α, β = 90°, γ = 120°, V = 6302.2(6) $Å^3$, Z = 12, D_{calc} = 1.298 $g{\cdot}cm^{-3}$, μ(Mo-K_α) = 0.104 mm^{-1}, 1091 refinement parameters, 19,346 reflections measured, 7909 unique reflections, which were used in all calculations. The final R was 0.071. The Cambridge Crystallographic Data Centre (CCDC) 1857049 contains the supplementary crystallographic data for this compound.

A single crystal of compound **3e** was obtained by crystallization from chloroform:hexane – 1:1. The X-ray studies were performed as described above for compound **3f**. Main crystallographic data for **3e**: $C_{21}H_{23}F_3N_2O_3$, M = 408.41, space group $P\bar{1}$, triclinic, a = 9.6197(9), b = 9.7051(10), c = 11.3490(9) Å, α = 76.574(8)°, β = 75.999(8)°, γ = 77.041(9)°, V = 983.99(16) $Å^3$, Z = 2, D_{calc} = 1.378 $g{\cdot}cm^{-3}$, μ(Mo-K_α) = 0.111 mm^{-1}, 292 refinement parameters, 6309 reflections measured, 2649 unique reflections, which were used in all calculations. The final R was 0.052. CCDC 1857050 contains the supplementary crystallographic data for this compound.

Crystal structures were solved by direct methods followed by Fourier synthesis with SHELXS-97 [36] and refined with full-matrix least-squares methods for all non-hydrogen atoms with the SHELXL-97 software packages [36].

2.3. Synthesis of compounds

Synthesis of lithium salts 2a-j. A mixture of ethyl 4,4,4-trifluoro-3-oxobutanoate **1** (40 mmol) and the corresponding alcohol (40 mmol) in toluene (100 ml) was refluxed with a Dean-Stark receiver for 24 h. The solvent was removed *in vacuo*. The residue was dissolved in hexane (100 ml), then LiH (40 mmol) was added. The mixture was refluxed for 24 h and the solvent was removed. The resulting lithium salt **2a-c** was washed with ether and hexane, and recrystallized fractionally from toluene. The salts **2d-j** were used without further purification in the ensuing reactions.

Lithium 1,1,1-trifluoro-4-hexyloxy-4-oxobut-2-en-2-olate (2a). Yield 72%, white powder. ^{1}H NMR (DMSO-d_6): δ 0.86 (m, 3H, Me), 1.27 (m, 4H, 2CH_2), 1.53 (m, 2H, CH_2), 3.93 (t, 2H, OCH_2, J 6.7 Hz), 4.78 (s, 1H, CH). ^{19}F NMR (DMSO-d_6): δ −75.1 (s, CF_3). Anal. calcd. for $C_{10}H_{14}F_3LiO_3$. C, 48.79; H, 5.73. Found: C, 48.63; H, 5.88.

Lithium 4-dodecyloxy-1,1,1-trifluoro-4-oxobut-2-en-2-olate (2b). Yield 75%, white powder. ^{1}H NMR (DMSO-d_6): δ 0.85 (m, 3H, Me), 1.24 (m, 18H, 9CH_2), 1.53 (m, 2H, CH_2), 3.93 (m, 2H, OCH_2), 4.79 (s, 1H, CH). ^{19}F NMR (DMSO-d_6): δ −75.1 (s, CF_3). Anal. calcd. for $C_{16}H_{26}F_3LiO_3$. C, 58.18; H, 7.93. Found: C, 58.32; H, 7.81.

Lithium 4-citronellyloxy-1,1,1-trifluoro-4-oxobut-2-en-2-olate (2c). Yield 80%, white powder. ^{1}H NMR (DMSO-d_6): δ 0.87 (d, 3H, Me, J 6.5 Hz), 1.14 (m, 1H, CH), 1.32 (m, 2H, CH_2), 1.49 (m, 1H, CH), 1.56 (s and m, 4H, Me and CH), 1.64 (s, 3H, Me), 1.94 (m, 2H, CH_2), 3.98 (m, 2H, OCH_2), 4.79 (s, 1H, =CH), 5.08 (unsolv t, 1H, =CH_{Alk}, J 7.1 Hz). ^{19}F NMR (DMSO-d_6): δ −75.1 (s, CF_3). Anal. calcd. for $C_{14}H_{20}F_3LiO_3$. C, 56.00; H, 6.71. Found: C, 56.12; H, 6.80.

Synthesis of arylhydrazones 3a-j. The azo coupling reaction was performed by a standard procedure [37]. The yields of arylhydrazones **3d-j** were based on the initial 3-oxoester **1**.

Hexyl (2*Z*)-4,4,4-trifluoro-2-[2-(4-methylphenyl)hydrazinylidene]-3-oxobutanoate (3a). Yield 68%, orange oil (eluent – chloroform:hexane, 3:1). IR (FTIR): ν 2921, 1595 (NH), 1715 (CO_2Et), 1677 (C=O), 1530 (C=C, C=N), 1209–1190 (C−F) cm^{-1}. ^{1}H NMR (DMSO-d_6): δ 0.88 (t, 3H, Me, J 7.0 Hz), 1.30, 1.40, 1.68 (all m, 6H, 3CH_2), 2.32 (s, 3H, C_6H_4−*Me*), 4.29 (t, 2H, OCH_2, J 6.5 Hz), 7.28, 7.47 (both d, 4H, C_6H_4, J 8.3 Hz), 13.00 (s, 1H, NH). ^{19}F NMR (DMSO-d_6): δ −69.5 (s, CF_3). Anal. calcd. for $C_{17}H_{21}F_3N_2O_3$. C, 56.98; H, 5.91; N, 7.82. Found: C, 56.87; H, 5.99; N, 7.92.

Dodecyl (2*Z*)-4,4,4-trifluoro-2-[2-(4-methylphenyl)hydrazinylidene]-3-oxobutanoate (3b). Yield 65%, orange oil (eluent – chloroform : hexane, 2:1). IR (FTIR): ν 2926, 1594 (NH), 1714 (CO_2Et), 1675 (C=O), 1528 (C=C, C=N), 1208–1193 (C−F) cm^{-1}. ^{1}H NMR (DMSO-d_6): δ 0.84 (t, 3H, Me, J 6.9 Hz), 1.28 (m, 16H, 8CH_2), 1.39, 1.68 (both m, 4H, 2CH_2), 2.31 (s, 3H, C_6H_4−*Me*), 4.28 (t, 2H, OCH_2, J 6.5 Hz), 7.28, 7.46 (both d, 4H, C_6H_4, J 8.3 Hz), 12.99 (s, 1H, NH). ^{19}F NMR (DMSO-d_6): δ −69.5 (s, CF_3). Anal. calcd. for $C_{23}H_{33}F_3N_2O_3$. C, 62.43; H, 7.52; N, 6.33. Found: C, 62.52; H, 7.37; N, 6.28.

Citronellyl (2*Z*)-4,4,4-trifluoro-2-[2-(4-methylphenyl)hydrazinylidene]-3-oxobutanoate (3c). Yield 70%, orange oil (eluent – chloroform : hexane, 2:1). IR (FTIR): ν 2926, 1594 (NH), 1717 (CO_2Et), 1670 (C=O), 1533 (C=C, C=N), 1208–1191 (C−F) cm^{-1}. ^{1}H NMR (DMSO-d_6): δ 0.92 (d, 3H, Me, J 6.6 Hz), 1.17 (m, 1H, CH), 1.34 (m, 1H, CH), 1.51 (m, 1H, CH), 1.55 (s, 3H, Me) 1.62 (s and m, 4H, Me and CH), 1.73 (m, 1H, CH), 2.31 (s, 3H, C_6H_4−*Me*), 1.96 (m, 2H, CH_2), 4.33 (m, 2H, OCH_2), 5.08 (m, 1H, =CH), 7.28, 7.47 (both d, 4H, C_6H_4, J 8.3 Hz), 13.01 (s, 1H, NH). ^{19}F NMR (DMSO-d_6): −69.5 (s, CF_3). ^{19}F NMR ($CDCl_3$): −71.6 (s, CF_3). Anal. calcd. for $C_{21}H_{27}F_3N_2O_3$. C, 61.15; H, 6.60; N, 6.79. Found: C, 61.22; H, 6.70; N, 6.68.

Geranyl (2*Z*)-4,4,4-trifluoro-2-[2-(4-methylphenyl)hydrazinylidene]-3-oxobutanoate (3d). Yield 71%, orange oil (eluent – chloroform : hexane, 2:1). IR (FTIR): ν 2925, 1594 (NH), 1714 (CO_2Et), 1675 (C=O), 1533 (C=C, C=N), 1207–1190 (C−F) cm^{-1}. ^{1}H NMR (DMSO-d_6): δ 1.55, 1.62, 1.73 (all s, 9H, 3 Me), 2.05 (m, 4H, 2CH_2), 2.31 (s, 3H, C_6H_4−*Me*), 4.83 (d, 2H, OCH_2, J 7.0 Hz), 5.06 (t, 1H, $C^{2'}H$, J 5.9 Hz), 5.40 (t, 1H, $C^{6'}H$, J 6.7 Hz), 7.28, 7.47 (both d, 4H, C_6H_4, J 8.3 Hz), 13.00 (s, 1H, NH). ^{19}F NMR (DMSO-d_6): −69.5 (s, CF_3). ^{19}F NMR ($CDCl_3$): −71.5 (s, CF_3). Anal. calcd. for $C_{21}H_{25}F_3N_2O_3$. C, 61.45; H, 6.14; N, 6.83. Found: C, 61.57; H, 6.02; N, 6.69.

Adamantyl (2*Z*)-4,4,4-trifluoro-2-[2-(4-methylphenyl)hydrazinylidene]-3-oxobutanoate (3e). Yield 65%, yellow crystals, mp 159–160 °C (eluent – chloroform:hexane, 1:1). IR (FTIR): ν 2923, 1591 (NH), 1712 (CO_2Et), 1670 (C=O), 1530 (C=C, C=N), 1208–1193 (C−F) cm^{-1}. ^{1}H NMR (DMSO-d_6): δ 1.66, 2.20 (both br.s, 15H, adamantyl), 1.73 (m, 1H, CH), 2.31 (s, 3H, C_6H_4−*Me*), 7.28, 7.48 (both d, 4H, C_6H_4, J 8.4 Hz), 13.05 (s, 1H, NH). ^{19}F NMR (DMSO-d_6): −69.4 (s, CF_3). Anal. calcd. for $C_{21}H_{23}F_3N_2O_3$. C, 61.76; H, 5.68; N, 6.86. Found: C, 61.86; H, 5.72; N, 6.79.

Bornyl (2*Z*)-4,4,4-trifluoro-2-[2-(4-methylphenyl)hydrazinylidene]-3-oxobutanoate (3f). Yield 78%, light-yellow powder, mp 94–95 °C (eluent – chloroform:hexane, 2:1). IR (FTIR): ν 2964, 1595 (NH), 1706 (CO_2Et), 1667 (C=O), 1520 (C=C, C=N), 1204–1183 (C−F) cm^{-1}. ^{1}H NMR (DMSO-d_6): δ 0.87, 0.89, 0.92 (all s, 9H, 3Me), 1.14 (dd, 1H, CH, J 13.8, 3.4 Hz), 1.25 (m, 1H, CH), 1.33 (m, 1H, CH), 1.73 (m, 2H, CH_2), 2.17 (m, 1H, CH), 2.32 (s, 3H, C_6H_4−*Me*), 2.36 (m, 1H, CH), 5.01 (ddd, 1H, OCH, J 9.8, 3.2, 2.3 Hz), 7.28, 7.48 (both d, 4H, C_6H_4, J 8.1 Hz), 13.16 (s, 1H, NH). ^{19}F NMR (DMSO-d_6): −69.4 (s, CF_3). ^{19}F NMR ($CDCl_3$): −71.5 (s, CF_3). Anal. calcd. for $C_{21}H_{25}F_3N_2O_3$. C, 61.45; H, 6.14; N, 6.83. Found: C, 61.52; H, 6.19; N, 6.88.

Isobornyl (2*Z*)-4,4,4-trifluoro-2-[2-(4-methylphenyl)hydrazinylidene]-3-oxobutanoate (3 g). Yield 73%, light-yellow oil (eluent – chloroform:hexane, 2:1). IR (FTIR): ν 2952, 1593 (NH), 1711 (CO_2Et), 1667 (C=O), 1533 (C=C, C=N), 1209–1191 (C−F) cm^{-1}. ^{1}H NMR (DMSO-d_6): δ 0.84, 0.91, 1.02 (all s, 9H, 3Me), 1.14 (m, 2H, CH_2), 1.58 (m, 1H, CH), 1.70 (m, 1H, CH), 1.76 (m, 1H, CH), 1.86 (m, 1H, CH), 2.17 (m, 1H, CH), 2.32 (s, 3H, C_6H_4−*Me*), 4.81 (dd, 1H, OCH, J 7.3, 4.1 Hz), 7.28, 7.48 (both d, 4H, C_6H_4, J 8.3 Hz), 13.16 (s, 1H, NH). ^{19}F NMR (DMSO-d_6): −69.4 (s, CF_3). ^{19}F NMR ($CDCl_3$): −71.6 (s, CF_3). Anal. calcd. for $C_{21}H_{25}F_3N_2O_3$. C, 61.45; H, 6.14; N, 6.83. Found: C, 61.60; H, 6.25; N, 6.77.

L-Menthyl (2*Z*)-4,4,4-trifluoro-2-[2-(4-methylphenyl)hydrazinylidene]-3-oxobutanoate (3 h). Yield 70%, orange oil (eluent – chloroform:hexane, 2:1). IR (FTIR): ν 2959, 2982, 1594 (NH), 1717 (CO_2Et), 1665 (C=O), 1532 (C=C, C=N), 1209–1191 (C−F) cm^{-1}. ^{1}H NMR (DMSO-d_6): δ 0.73 (d, 3H, Me, J 6.9 Hz), 0.89 (m, 7H, 2 Me and CH), 1.07 (m, 2H, CH_2), 1.48 (m, 2H, CH_2), 1.66 (m, 2H, CH_2), 2.07 (m, 2H, CH_2), 2.32 (s, 3H, C_6H_4−*Me*), 4.82 (td, 1H, OCH, J 10.8, 4.2 Hz), 7.29, 7.49 (both d, 4H, C_6H_4, J 8.2 Hz), 13.12 (s, 1H, NH). ^{19}F NMR (DMSO-d_6): −69.5 (s, CF_3). ^{19}F NMR ($CDCl_3$): −71.5 (s, CF_3). Anal. calcd. for $C_{21}H_{27}F_3N_2O_3$. C, 61.15; H, 6.60; N, 6.79. Found: C, 61.26; H, 6.65; N, 6.72.

DL-Menthyl (2*Z*)-4,4,4-trifluoro-2-[2-(4-methylphenyl)hydrazinylidene]-3-oxobutanoate (3i). Yield 70%, orange oil (eluent – chloroform:hexane, 2:1). IR (FTIR): ν 2959, 2982, 1594 (NH), 1717 (CO_2Et), 1665 (C=O), 1533 (C=C, C=N), 1209–1191 (C−F) cm^{-1}. ^{1}H NMR (DMSO-d_6): δ 0.73 (d, 3H, Me, J 6.9 Hz), 0.88 (m, 7H, 2 Me and CH), 1.06 (m, 2H, CH_2), 1.47 (m, 2H, CH_2), 1.66 (m, 2H, CH_2), 2.05 (m, 2H, CH2), 2.32 (s, 3H, C_6H_4−*Me*), 4.81 (td, 1H, OCH, J 10.9, 4.3 Hz), 7.28, 7.50 (both d, 4H, C_6H_4, J 8.4 Hz), 13.14 (s, 1H, NH). ^{19}F NMR (DMSO-d_6): −69.5 (s, CF_3). Anal. calcd. for $C_{21}H_{27}F_3N_2O_3$. C, 61.15; H, 6.60; N, 6.79. Found: C, 61.19; H, 6.72; N, 6.70.

Cholesteryl (2*Z*)-4,4,4-trifluoro-2-[2-(4-methylphenyl)hydrazinylidene]-3-oxobutanoate (3j). Yield 60%, orange powder, mp 179–180 °C (eluent – chloroform:hexane, 2:1). IR (FTIR): ν 2946, 2869, 1595 (NH), 1707 (CO_2Et), 1668 (C=O), 1533 (C=C, C=N), 1210–1189 (C−F) cm^{-1}. ^{1}H NMR ($CDCl_3$): δ 0.69 (br.s, 3H, Me), 0.87 (dd, 6H, 2Me, J 6.6, 2.2 Hz), 0.92 (d, 3H, Me, J 6.5 Hz), 1.06 (s, 3H, Me), 1.00, 1.33, 1.51 (all m, 20H, set of CH and CH_2 group of cholesteryl moiety), 1.83 (m, 2H, CH_2), 1.99 (m, 4H, 2 CH_2), 2.37 (s, 3H, C_6H_4−*Me*), 2.45, 2.53 (both m, 2H, 2 CH), 4.82 (m. 1H, OCH), 5.42 (m, 1H, =CH), 7.23, 7.31 (both d, 4H, C_6H_4, J 8.4 Hz), 13.51 (s, 1H, NH). ^{19}F NMR ($CDCl_3$): −71.6 (s, CF_3). Anal. calcd. for $C_{38}H_{53}F_3N_2O_3$. C, 71.00; H, 8.31; N, 4.36. Found: C, 71.12; H, 8.40; N, 4.28

2.4. Biological assays

2.4.1. Enzyme assays

2.4.1.1. Inhibition in vitro of porcine liver CES, hCES1, hCES2, AChE, and BChE. The following enzymes were purchased from Sigma-Aldrich: human erythrocyte acetylcholinesterase (AChE, EC 3.1.1.7), equine serum butyrylcholinesterase (BChE, EC 3.1.1.8), porcine liver carboxylesterase (CES, EC 3.1.1.1) and human recombinant carboxylesterases hCES1 (E0287, Carboxylesterase 1 isoform b human

recombinant, expressed in baculovirus infected BTI insect cells) and hCES2 (E4749, Carboxylesterase 2 human recombinant, expressed in mouse NSO cells, ≥95% (SDS-PAGE)).

Substrates for AChE, BChE, and CES were acetylthiocholine iodide (ATCh), butyrylthiocholine iodide (BTCh), and 4-nitrophenol acetate (4-NPA), respectively, and the colorimetric reagent for the AChE and BChE assays was 5,5′-dithio-bis-(2-nitrobenzoic acid) (DTNB) (Sigma-Aldrich).

Ellman's colorimetric assay was used to measure AChE and BChE activities in 0.1 M K/Na phosphate buffer at pH 7.5, 25 °C [38]. Final concentrations of reactants were 0.33 mM DTNB, 0.02 unit/mL of AChE or BChE and 1 mM of substrate (ATCh or BTCh, respectively). Reagent blanks consisted of reaction mixtures without enzymes to assess non-enzymatic hydrolysis of substrates.

CES (porcine liver) activity was assessed colorimetrically in 0.1 M K/Na phosphate buffer pH 8.0, 25 °C, by measuring the absorbance of 4-nitrophenol at 405 nm [39]. Final enzyme and substrate (4-NPA) concentrations were 0.02 unit/mL and 1 mM, respectively. Reagent blanks included all constituents except enzyme.

Activities of hCES1 and hCES2 were determined in the same manner as porcine liver CES [39], except that the final concentration of hCES2 was 0.01 unit/mL. Again, blanks consisted of all reagents except the enzymes.

Test compounds were dissolved in DMSO. Reaction mixtures contained a final DMSO concentration of 2% (v/v). This concentration of DMSO on its own did not significantly affect the activity of any of the enzymes in the study (data not shown).

Enzyme inhibition was first assessed at a single concentration of 20 μM for each compound after a 5 min incubation at 25 °C in three separate experiments. The most active compounds were then selected for determination of the IC_{50} (inhibitor concentration resulting in 50% inhibition of control enzyme activity). Compounds (eight concentrations between 10^{-12} and 10^{-4} M were selected to achieve 20 to 80% inhibition) were incubated with each enzyme for 5 min at 25 °C. Substrate was then added and residual enzyme activity relative to an inhibitor-free control was measured using a Bio-Rad Benchmark Plus microplate spectrophotometer. Origin 6.1 for Windows was used to determine IC_{50} values from plots of log (inhibitor concentration) vs. % (residual activity). Results were expressed as mean ± SEM ($n = 3$ experiments).

2.4.1.2. Porcine liver CES inhibition kinetics: Inhibition constants at steady state. Mechanisms of inhibition were assessed for the five most active compounds against porcine liver CES. Residual activity was measured following 5 min incubation at 25 °C with three increasing concentrations of inhibitor and six decreasing substrate concentrations – substrate was added immediately after the 5 min incubation with inhibitor and rates of absorption of 4-nitrophenol production were monitored at 405 nm using a Bio-Rad Benchmark Plus microplate spectrophotometer. Inhibition constants K_i (competitive component) and αK_i (noncompetitive component) were determined by linear regression of 1/V versus 1/[S] double-reciprocal (Lineweaver-Burk) plots using Origin 6.1 for Windows. Data were expressed as mean ± SEM ($n = 3$ experiments).

2.4.2. ABTS radical cation scavenging assay as a measure of antioxidant activity

Antioxidant activity of compounds was determined by the ability of the compounds to decolorize the $ABTS^{\bullet+}$ radical cation as previously described [40], incorporating modifications described below. This method measures the relative ability of antioxidant compounds to scavenge the radical cation 2,2′-azinobis-(3-ethylbenzothiazoline-6-sulfonic acid) ($ABTS^{\bullet+}$) compared with a standard amount of the synthetic antioxidant Trolox (6-hydroxy-2,5,7,8-tetramethylchroman-2-carboxylic acid), a vitamin E analogue. The assay is based on the generation and detection of a colored long-lived specific radical cation, $ABTS^{\bullet+}$.

Tokyo Chemical Industry Co., Ltd. was the source of ABTS. Potassium persulfate (di-potassium peroxydisulfate), Trolox®, ascorbic acid, and ethanol (HPLC grade) were purchased from Sigma-Aldrich. Deionized water was used to prepare aqueous solutions.

Stock solutions of antioxidant standards included Trolox, ascorbic acid, and catechol (5 mM) in DMSO. Working solutions (1–100 μM) were freshly prepared on the day of experiments to serve as calibrants and positive controls for $ABTS^{\bullet+}$ scavenging activity.

ABTS radical cation ($ABTS^{\bullet+}$) was produced by mixing equal volumes of 7 mM ABTS stock solution in deionized water with 2.45 mM aqueous potassium persulfate solution and permitting the reaction to proceed at room temperature in the dark for 12–16 h. The absorbance at 734 nm of the resulting $ABTS^{\bullet+}$ solution was adjusted to 0.80 ± 0.05 by diluting with HPLC-grade ethanol.

Radical scavenging activity of compounds was determined by measuring the decrease in absorbance at 734 nm 1 h after mixing 10 μl of test compound solution with 240 μl of $ABTS^{\bullet+}$ working solution using a Bio-Rad xMark microplate UV/VIS spectrophotometer vs. ethanol blanks. Antioxidant activity was expressed as Trolox equivalent antioxidant capacity (TEAC) values (ratios between slopes of linear correlations for concentrations of test compounds and Trolox with absorbance of the ABTS radical). IC_{50} values (concentrations required to reduce 50% of the ABTS radical) were determined for the most active compounds via linear regression using Origin 6.1 for Windows; data are reported as mean ± SEM based on triplicate replicates and $n = 3$ experiments.

2.4.3. Acute toxicity studies

2.4.3.1. Animals. Adult male CD-1 mice were obtained from the Animal Unit "Pushchino" at the M.M. Shemyakin and Yu.A. Ovchinnikov Institute of Bioorganic Chemistry RAS (Russia). Animals were kept in groups of three in polypropylene "shoebox" cages (Bioskape) with standard bedding (Rehofix MK 2000, J. Rettenmaier & Söhne) and supplied *ad libitum* with feed (Chara, "Assortiment-Agro", Russia) and tap water. The animal facility provided a climate-controlled 12 h light: 12 h dark light cycle. Russian Federal Law № 61-FZ [41] and guidelines for preclinical study of medicinal products [42] were observed for the care and procedures with animal subjects.

2.4.3.2. Evaluation of acute toxicity. Evaluation of acute toxicity was carried out using adult male CD-1 mice based on OECD recommendations [43] and guidelines for preclinical study of medicinal products [42]. Test compounds were injected intraperitoneally (i.p.), three mice per dose level, at doses of 100 and 300 mg/kg in 2% (w/v) starch mucilage solution [42]. The post-dosing observation period was 14 days with determination of the number of survived animals.

2.5. Molecular modeling studies

2.5.1. Structure preparation

Initial structures of possible enantiomers and tautomers of inhibitors were prepared with MarvinSketch 14.9.1.0 (ChemAxon, http://www.chemaxon.com). Quantum mechanical (QM) optimization of the generated structures was performed with GAMESS-US [44] using DFT method (B3LYP/6-31G*). Obtained geometries of the ligands were used for following molecular docking. Partial atomic charges on ligand atoms were assigned from QM data according to the Mulliken scheme [45].

Protein structure of hCES1 for molecular docking was prepared using chain A of the X-ray structure PDB: 2H7C [46] (hCES; 2.00 Å resolution) as described in our previous docking study with this enzyme [47].

The human CES2 (hCES2) (Uniprot: O00748) and porcine CES (CES1) (Uniprot: Q29550) homology models were built by Modeller

v9.14 software [48] using the human CES (CES1) X-ray structure (PDB: 2H7C) as a template. Quality of the obtained structures was checked with the MolProbity webserver [49] and found to be close to the quality of the initial X-ray structure. For optimization of the both homology models, they were solvated in TIP3P water (rectangular box with borders extending 10 Å from the protein) and counterions added so that the final concentrations of Na^+ and Cl^- were 0.15 M. The solvated systems were energy-minimized during 5000 steps with the protein backbone atoms fixed, than subjected to 10 ns MD simulation (NPT ensemble, 298 K) with harmonic constraints on backbone atoms. Finally, to mimic crystallization conditions, the systems were cooled down to 4 K during 29 ns and energy minimized without constraints. MD simulations were performed with NAMD 2.10 [50] and the CHARMM36 force field [51] using the Lomonosov supercomputer [52].

2.5.2. Molecular docking

Molecular docking with a Lamarckian Genetic Algorithm (LGA) was performed with Autodock 4.2.6 software [53,54]. The grid box included the entire CES active site and gorge with dimensions 22.5 Å × 22.5 Å × 22.5 Å and a grid spacing of 0.375 Å. The main selected LGA parameters were 256 runs, 25×10^6 evaluations, 27×10^4 generations, and population size 300. Structural images were prepared with PyMOL (https://pymol.org/).

2.6. ADMET profile predictions

ADMET profile predictions were based on computational methods for human intestinal absorption (HIA) [55], blood-brain barrier permeability (LogBB) [56], and hERG-mediated cardiac toxicity risk (channel affinity pK_i and inhibitory activity pIC_{50}) [57]. Calculations were carried out by the integrated online service for ADMET properties prediction [58]. This web server incorporates accurate and representative training sets, fragmental descriptors, and artificial neural networks into its predictive QSAR models.

2.7. Statistical analyses

Results are presented as mean ± SEM calculated using GraphPad Prism version 6.05 for Windows. Plots, linear regressions, and IC_{50} values were determined using Origin 6.1 for Windows, OriginLab (Northampton, MA).

3. Results and discussion

3.1. Chemistry

Transesterification is one of the more convenient procedures for the synthesis of commercially unavailable 3-oxo esters, which are used in the synthesis of polymers, drugs, and many others compounds [59]. A transesterification reaction is more advantageous than the Claisen condensation or the reaction of diketene with alcohols for the synthesis of such 3-oxo esters [60].

Two main approaches for transesterification are known. One of them is based on an application of various catalysts such as inorganic salts (Cs_2CO_3 [61], $MnSO_4$ [62], $MnCO_3$ [62], $LiClO_4$ [63], $SmCl_3$ [64]), organic bases (Et_3N [60], 4-dimethylaminopyridine [65,66]) and complexes ([N,N'-ethylene bis(salicylideneaminato)]manganese(III) chloride, vanadyl(IV) acetate [67], ytterbium(III) triflate [68], and distannoxanes [X(*n*-Bu)$_2$Sn-O-Sn(*n*-Bu)$_2$OH (X = Cl, SCN)]) [69]. Transesterification of methyl/ethyl 3-oxo esters with primary, secondary, allylic, cyclic and benzylic alcohols has been carried out in moderate to good yields under solvent-free conditions using borate zirconia solid acid (B_2O_3/ZrO_2) catalyst [70]. An analogous type of reaction involves transesterification of copper(II) chelates of polyfluoroalkyl-containing 3-oxo esters with borneol [71], and naturally occurring clays efficiently catalyze transesterification of 3-oxo esters with carbohydrate derivatives [72]. However, in spite of the potential utility of these methods, most of them experienced various disadvantages such as harsh reaction conditions, modest yields, special experimental apparatus requirements, and the use of expensive, toxic, or air-sensitive catalysts.

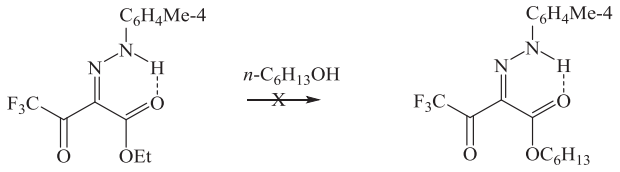

Scheme 1. Unsuccessful transesterification of ethyl 4,4,4-trifluoro-2-tolylhydrazinylidene-3-oxobutanoate with *n*-hexanol.

In contrast, the catalyst-free alcoholysis of 3-oxo esters in refluxing toluene [60,63,73] or without solvent [74] is a simpler procedure. Using molecular sieves under these conditions promotes reaching yields of up to 95% [75]. Transesterified 3-oxo esters can be purified by distillation or column chromatography, but more often they may be used in subsequent syntheses without further purification that could lead to reducing the yield of the target compounds.

Our attempts to carry out the transesterification of ethyl 4,4,4-trifluoro-2-tolylhydrazinylidene-3-oxobutanoate with *n*-hexanol in the presence of Et_3N or metal salts and without catalyst were unsuccessful (Scheme 1).

However, the transesterification of ethyl trifluoroacetylacetate **1** with *n*-hexanol proceeds equally well, both in the presence and absence of Et_3N catalyst. Therefore, the reaction of ester **1** with other alcohols has been carried out in toluene with azeotropic distillation of ethanol under catalyst-free conditions (Scheme 2). In addition, dodecanol, citronellol, geraniol, borneol, isoborneol, L-menthol, DL-menthol, adamantol, and cholesterol were used as alcoholic components in the syntheses. The transesterified esters were isolated as lithium salts **2a-j**.

Lithium salts of oxo esters **2a-c** were isolated as pure substances followed by azo coupling with tolyldiazonium chloride that allowed us to obtain the target 2-tolylhydrazonylidene-3-oxo esters **3a-c** (Scheme 2). It was found that lithium salts **2** could be involved in the subsequent synthesis without additional purification. As a result, a series of 3-oxo-2-tolylhydrazinylidene-4,4,4-trifluorobutanoates **3a-j** bearing various higher and natural alcohol moieties were obtained.

According to X-ray analysis, 2-tolylhydrazinylidene-3-oxo esters **3e,f** exist in crystals as *Z*–isomers (Figs. 1, 2). Each of these isomers is stabilized by an intramolecular hydrogen bond between the hydrogen atom on the NH group of the hydrazine fragment and the oxygen atom of the alkoxycarbonyl moiety. Thus, for ester **3e**, the intramolecular distance $N^1H^1\ldots O^2$ is 1.92(1) Å, with bond angles $N^1H^1O^2$ and $C^1O^2H^1$ of 136(1) and 98.1(5)°, and for ester **3f**, the intramolecular hydrogen bond distance is 2.06(3) Å, with bond angles $N^2H^2O^3$ and $C^1O^3H^2$ of 132(4) and 99(1)°, respectively. Moreover, there is a *s-cis,s-trans* conformation of the *Z*-isomer in crystals of esters **3e,f**, such that the trifluoromethyl and alkoxyl substituents are located in the *trans*-position relative to C(=O)−C(=NNHAr)−C(=O).

The equivalence of the IR spectra of compounds **3e,f**, measured in the solid state and in chloroform solution indicates that they exist as *Z*-isomers both in solution and in crystals. The NMR spectra of esters **3a-j** have one set of signals. Thus, the ^{19}F NMR spectra are characterized by the same chemical shifts of the CF_3 group (δ_F −69.4… −69.5 ppm in DMSO-d_6 and −71.5… −71.6 ppm in $CDCl_3$). The IR spectra also have similar characteristic carbonyl group vibrations (ν_{CO} 1706–1717, 1665–1677 cm^{-1}). Accordingly, the new 2-tolylhydrazinylidene-3-oxo esters **3a-j** exist both in crystals and in solutions as *s-cis,s-trans-Z*-isomers, analogously to methyl(ethyl) 2-arylhydrazonylidene-3-polyfluoroalkyl-3-oxopropionates studied earlier [76]. It is obvious that introduction of bulky alkoxyl substituents does not influence the aforementioned structural aspects of these compounds.

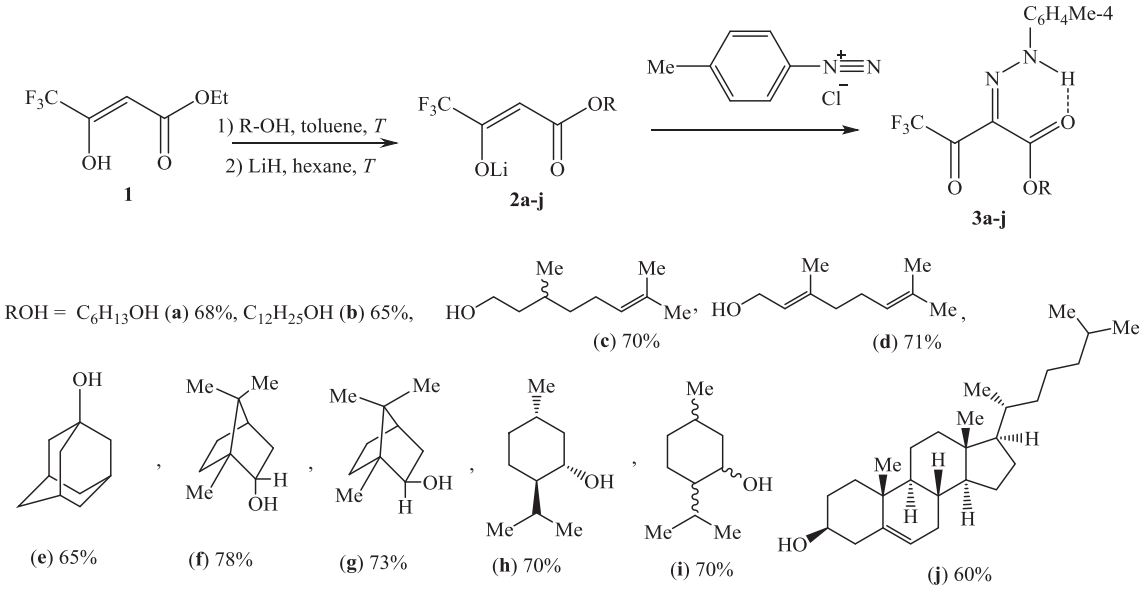

Scheme 2. Transesterification of ester **1** with alcohols to yield **2a-j** and further azo coupling to yield **3a-j**.

3.2. Inhibition studies of CES, AChE and BChE. Structure-activity relationships

The inhibitory potencies of the synthesized compounds against several serine esterases (i.e., an esterase profile) were determined using the commercially available enzymes: porcine liver carboxylesterase (EC 3.1.1.1, CES), human erythrocyte acetylcholinesterase (EC 3.1.1.7, AChE) and equine serum butyrylcholinesterase (EC 3.1.1.8, BChE) (Sigma, USA). AChE from human erythrocytes was used along with two enzymes of non-human origin, because of their relatively low cost and the exploratory character of this work. The high protein sequence identities between human and equine BChE (90%) and human CES1 and porcine liver CES (77%) [77] along with our previous results [47,77,78] demonstrated the applicability of this set of enzymes for determining the esterase profiles of new compounds.

Compounds **3a,c-i** were assessed for their potential to inhibit CES, AChE and BChE by determining the IC_{50} – the inhibitor concentration that decreases the enzyme activity by half. Bis-(4-nitrophenyl) phosphate (BNPP), which is a selective CES inhibitor, was used as a positive control. Compounds **3b,j** were found to be insoluble under the experimental conditions; therefore, their esterase profile was not determined.

The data characterizing the esterase profile of 3-oxo-2-tolylhydrazinylidene-4,4,4-trifluorobutanoates **3a,c-i** containing various fragments of higher or natural alcohols are shown in Table 1. All of the compounds were either weak inhibitors of cholinesterases or did not inhibit these enzymes. In contrast, the compounds were effective inhibitors of CES with IC_{50} values in the range from 0.013 to 0.092 μM. Thus, all of the studied 3-oxo-2-tolylhydrazonylidene-4,4,4-trifluorobutanoates **3a,c-i** were highly selective and effective inhibitors of porcine liver CES.

3.3. Kinetic studies of porcine CES inhibition

The most active compounds toward CES **3d-f** (Table 1) were selected for inhibition kinetics studies. Lineweaver-Burk plots – double reciprocal plots of Michaelis-Menten parameters – were used to evaluate the type of inhibition. The mechanism of inhibitory action for compounds **3d-f** toward CES is illustrated in Fig. 3. All the tested compounds were shown to be reversible CES inhibitors of mixed type. The values of CES inhibition constants (K_i – competitive component and αK_i – non-competitive component) are shown in Table 2.

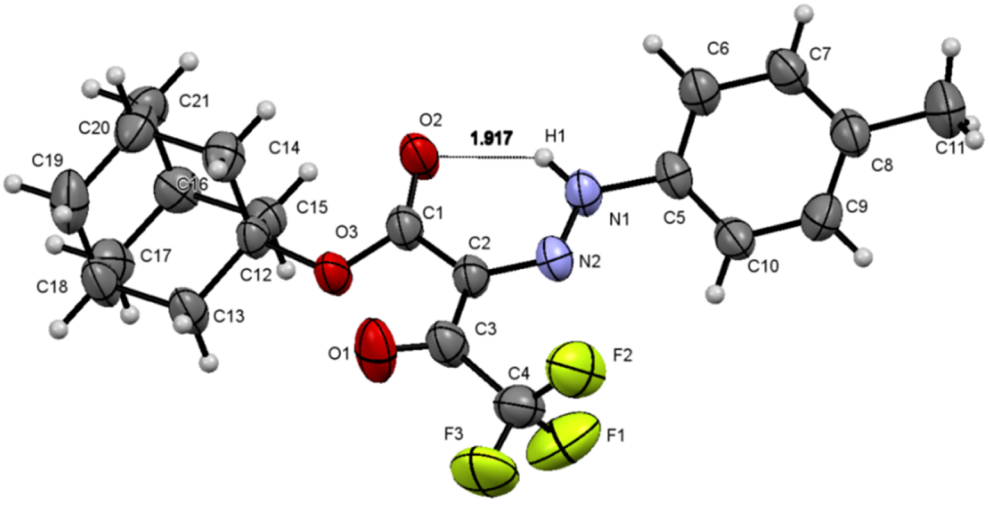

Fig. 1. ORTEP view of molecule **3e.**

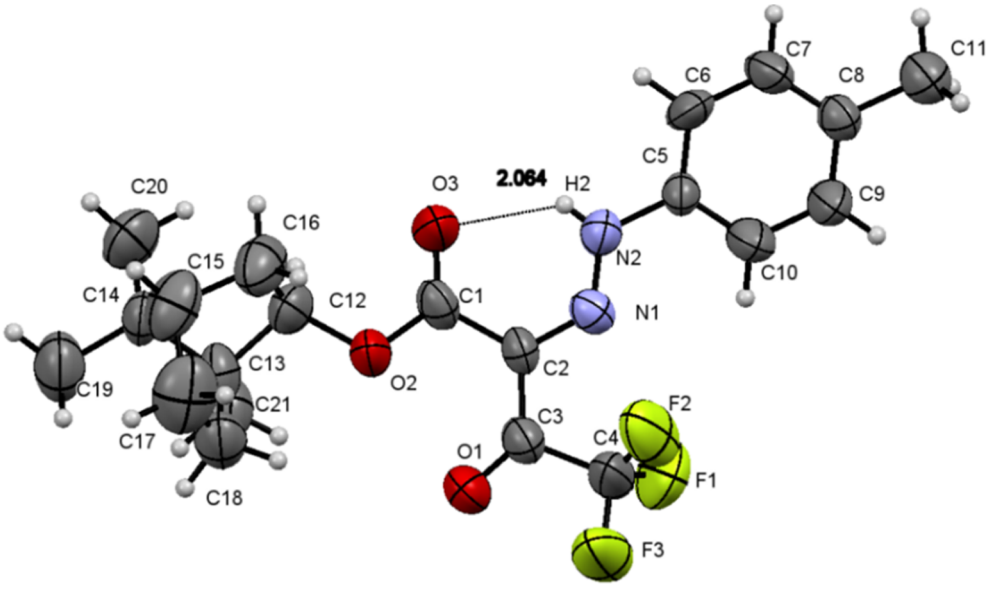

Fig. 2. ORTEP view of molecule **3f.**

3.4. Inhibition studies of hCES1 and hCES2. Structure-activity relationships

All of the studied compounds **3a,c-i** showed high activity and selectivity against porcine CES. Among these, the most active and selective compounds **3d-g** were studied as inhibitors of the main human isoenzymes involved in biotransformation of ester-containing drugs, hCES1 and hCES2.

Data on the inhibitory activity of these compounds toward hCES1 and hCES2 in comparison with their activity against porcine liver CES are presented in Table 3. The esters of geraniol (**3d**) and adamantol (**3e**) were highly active and selective inhibitors of hCES2, inhibiting this enzyme in the nanomolar range (IC_{50} = 0.00496 ± 0.00039 μM for **3d**

Table 1
The esterase profile and $ABTS^{\bullet+}$-scavenging activity of 3-oxo-2-tolylhydrazonylidene-4,4,4-trifluorobutanoates **3a,c-i.**

Compound	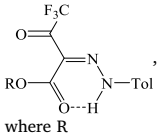 where R	Inhibitory activity IC_{50} ± SEM (μM) or inhibition % at 20 μM.			$ABTS^{\bullet+}$-scavenging	
		Porcine CES	Human AChE	Equine BChE	TEAC*	IC_{50}, μM
3a	*n*-C_6H_{13}	0.026 ± 0.002	8.4 ± 1.5%	51.3 ± 4.1	1.1 ± 0.06	16.5 ± 0.9
3c	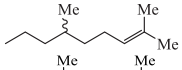	0.092 ± 0.007	n.a.	6.33 ± 1.1%	1.1 ± 0.07	17.3 ± 1.9
3d	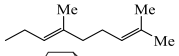	0.028 ± 0.002	n.a.	5.0 ± 1.4%	0.78 ± 0.06	26.5 ± 1.5
3e		0.013 ± 0.001	n.a.	3.1 ± 0.8%	0.86 ± 0.05	24.0 ± 1.1
3f	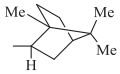	0.030 ± 0.003	n.a.	n.a.	0.96 ± 0.6	18.5 ± 1.3
3g	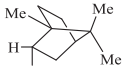	0.036 ± 0.003	n.a.	n.a.	0.95 ± 0.05	17.8 ± 1.0
3h	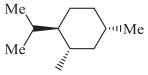	0.039 ± 0.003	n.a.	n.a.	0.96 ± 0.06	17.6 ± 1.4
3i	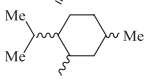	0.044 ± 0.003	n.a.	3.5 ± 0.9%	0.8 ± 0.04	18.2 ± 1.1
BNPP		1.80 ± 0.11	n.a.	n.a.	n.d.	n.d.
Trolox		n.d.	n.d.	n.d.	1.0	20.4 ± 0.8
Ascorbic acid		n.d.	n.d.	n.d.	0.98 ± 0.03	21.4 ± 2.3
Catechol		n.d.	n.d.	n.d.	1.2 ± 0.04	16.7 ± 1.2

Data are expressed as mean ± SEM, n = 3.
Esterase profiles: n.a. = not active at 20 μM.
Values expressed as % correspond to % inhibition at 20 μM.
Values without units of measurement correspond to IC_{50} values in μM.
n.d. = not determined.
* TEAC (Trolox equivalent antioxidant capacity) was determined from the ratio of the slopes of the concentration − response curves test compound/Trolox.

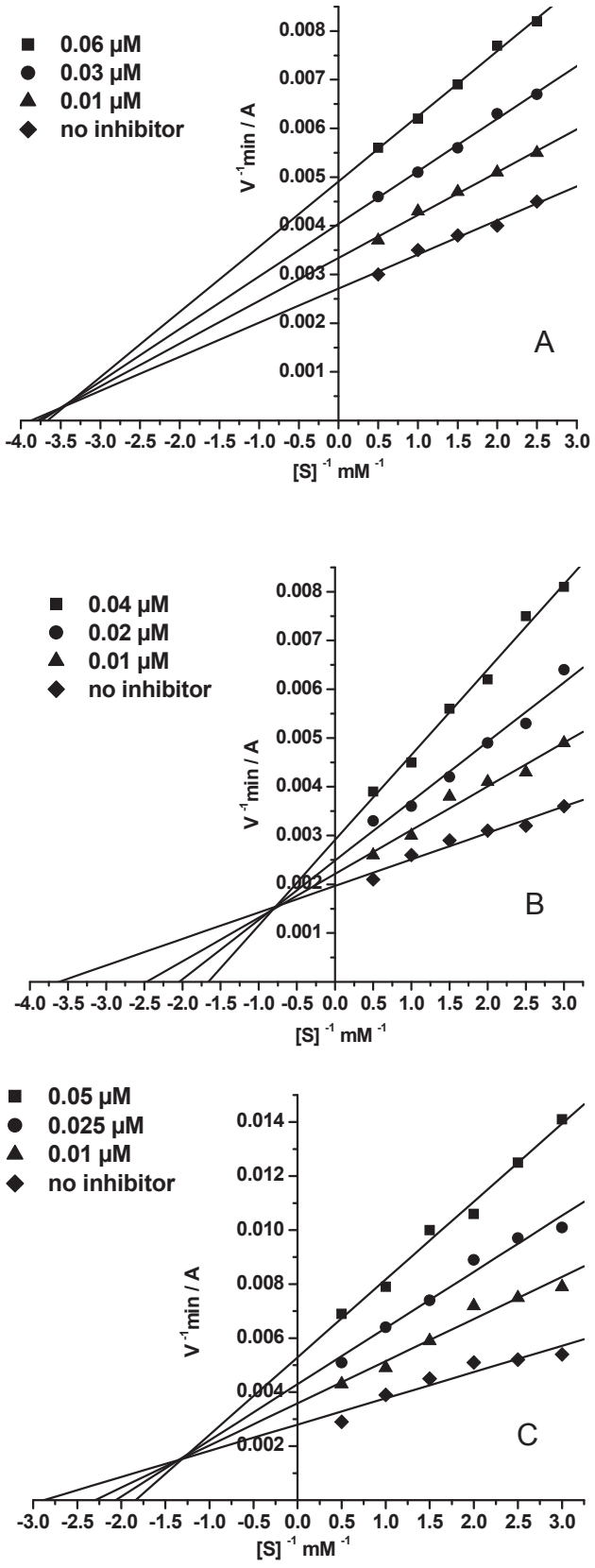

Fig. 3. Lineweaver-Burk double-reciprocal plots of steady state inhibition of porcine liver CES. (**A**) Compound **3d**. (**B**) Compound **3e**. (**C**) Compound **3f**. Each plot indicates mixed-type inhibition.

and IC_{50} = 0.00648 ± 0.00052 μM for **3e**). Moreover, these compounds were 10 times more selective toward hCES2 than hCES1.

In contrast, the esters of the stereoisomers of borneol (**3f**) and isoborneol (**3g**) were more active and selective against hCES1 than against hCES2. These compounds inhibited hCES1 with similar IC_{50} values of 0.098 ± 0.008 μM and 0.087 ± 0.007 μM, respectively. However, they had different inhibitory activities against hCES2, with IC_{50} values of 0.132 ± 0.012 μM for compound **3g** and 2.10 ± 0.18 μM for compound **3f**. Thus, the borneol ester **3f** was more selective toward hCES1 than the isoborneol ester **3g**.

It should be noted that unlike the inhibition of hCES2, the IC_{50} values of all the studied compounds toward hCES1 were in relatively consistent agreement with those obtained for porcine liver CES (Table 3). The IC_{50} selectivity ratios for hCES1/CES were in a comparatively narrow range of 1.9 to 4.5, whereas the hCES2/CES ratios varied widely from 0.18 to 70. The agreement between the hCES1 and porcine liver CES results is in accord with the high degree of protein sequence identity between these two enzymes. Thus, these results support the use of the less expensive porcine liver CES as a surrogate for hCES1 when carrying out preliminary evaluations of compounds intended to inhibit the human enzyme.

3.5. Molecular modeling studies

3.5.1. Quantum mechanics (QM) calculations

The 3-oxo-2-tolylhydrazinylidene-4,4,4-trifluorobutanoates **3** can exist in three tautomeric forms **I–III**, which may be *Z* and *E*-isomers. In addition, for the keto-azo-form **I** two enantiomers are possible (Scheme 3).

QM calculations were performed for all isomeric and tautomeric forms of compounds **3a,c-i**. The hydrazone tautomeric form **I** was found to be the most stable, while the keto-azo tautomer **II** was 10–14 kcal/mol less stable than **I**, and the keto-enol form **III** was 20–22 kcal/mol less stable than **I**. Both the *Z*- and *E*-isomers of the hydrazone tautomer **I** could be stabilized by intramolecular hydrogen bonds. For the *Z*-isomer, the hydrogen bond of the NH group of the hydrazine fragment with the single-bonded oxygen atom of the ester-group leads to weaker stabilization compared to the hydrogen bond with the carbonyl atoms in both the *Z*- and *E*-isomers. For all compounds **3a,c-i**, the *Z*-isomers were found to be more stable than the *E*–forms with energy differences of 0.04–0.7 kcal/mol (Fig. 4), which fully agrees with the X-ray data provided above. Therefore, based on X-ray crystallography and IR spectroscopy data, only the *Z*-isomers of the hydrazone tautomeric forms were used for molecular docking simulations.

3.5.2. Molecular docking into hCES1 and hCES2

Molecular docking studies were performed using the X-ray crystal structure of hCES1 (PDB: 2H7C) and a homology model of hCES2. Results for the keto-esters under consideration (**3a,c-i**) shared the same features: for all of them poses were found both inside and outside of the active site (Fig. 5A). Poses inside the catalytic active site were among the most favorable and resembled the position of esteratic substrates prior to hydrolysis, with the carbonyl oxygen of the trifluoromethyl-keto group in the oxyanion hole and its carbonyl carbon atom near the catalytic serine (Fig. 5B). This suggests the possibility of a chemical reaction between the enzyme and inhibitors. However, in the case of a trifluoromethyl-keto group in the active site, only the formation of a "transition state analog" [79] (in reality, a tetrahedral intermediate) without further hydrolysis is possible [32,80]. Poses of the compounds were also consistently found outside of the active site. Thus, these docking results correspond to the experimentally observed mixed type of inhibition.

Low sequence identity between hCES1 and hCES2 requires treating the hCES1 X-ray structure-based homology model of hCES2 with caution, but extensive MD optimization of the model performed by us helps

Table 2
The inhibition constants of porcine liver CES by the active compounds **3a,d-f**.[a]

Compound	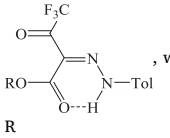 , where R	K_i (μM)	αK_i (μM)
3a	n-C_6H_{13}	0.0287 ± 0.0023	0.104 ± 0.009
3d	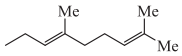	0.0731 ± 0.0066	0.122 ± 0.013
3e	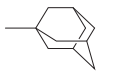	0.0218 ± 0.0019	0.0759 ± 0.0068
3f	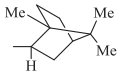	0.0271 ± 0.0024	0.0652 ± 0.0052

[a] Values for K_i (competitive inhibition constant) and αK_i (non-competitive inhibition constant) were determined from analyses of slopes of 1/V versus 1/S at various inhibitor concentrations. Values (means ± SEM) are from at least three separate experiments.

to reduce the influence of the template hCES1 structure on the homology model. Molecular docking of compounds **3d-g** shows differences in orientation of the compounds in the hCES2 active site, compared to the hCES1 results (see details in Appendix A), which helps to explain the experimentally observed differences in inhibitory activity.

3.5.3. Homology model of porcine CES

An X-ray crystal structure of porcine CES has recently been deposited in the PDB (PDB: 5FV4, resolution 2.4 Å). It is titled "Pig liver esterase 5", but the PDB file sequence is 100% identical to the sequence UniProt: A0A287BBZ0, *Sus scrofa* carboxylic ester hydrolase, gene *CES1*. However, use of this structure as a target for molecular docking does not lead to any binding pose in the active site of the enzyme. More detailed inspection of this X-ray structure revealed that the gorge leading from the protein surface to the active site is blocked by Phe286. Thus, the active site is a cavity that is isolated from the surface (Appendix A, Fig. S2). This makes this structure unsuitable for docking.

The use of homology models as docking targets has gained acceptance in recent years [81–83], and a human template has been used successfully to create homology models of non-human proteins as docking targets when suitable X-ray crystal structures were lacking [84]. Moreover, our current experimental results showing consistent inhibitory activity of compounds against human and porcine enzymes justify the use of human enzyme as a template for a porcine homology model for docking studies.

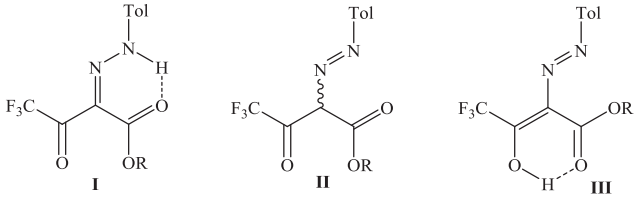

Scheme 3. Tautomeric forms of 3-oxo-2-tolylhydrazinylidene-4,4,4-trifluorobutanoates **3.**

Nevertheless, employment of a homology model of porcine CES has some caveats. For example, the use of the human CES1 X-ray structure as a template could introduce bias favoring the similarity of human and porcine docking results. To avoid this, we performed a molecular dynamics study to enable the protein to adopt a conformation determined by the porcine CES sequence rather than the template hCES1 structure.

3.5.4. Molecular docking into the porcine CES homology model

Docking results obtained with the optimized homology model structure of porcine CES exhibited slightly more diverse binding poses than for hCES1. In the case of porcine CES, all keto-ester inhibitors exhibited preferential binding to the active site, with the carbonyl oxygen atom of the esteratic group in the oxyanion hole (Fig. 6). In contrast, for hCES1, the carbonyl oxygen atom of the trifluoromethylketo group was found in the oxyanion hole (Fig. 5B). In spite of this difference, general orientations of the inhibitors in the catalytic active site were similar for both enzymes. However, orientation of the esteratic group relative to the catalytic residues did not support the possibility of a hydrolysis reaction: although formation of a tetrahedral intermediate would be possible, ether oxygen atom was too far from the catalytic histidine, and separated by the catalytic serine. This excludes the possibility of dissociation of the tetrahedral intermediate *via* the hydrolysis pathway but allows the reverse reaction if the tetrahedral product is not stable enough [32,80]. As was the case with the human enzyme, poses outside of the active site of porcine CES were also observed.

3.6. Antioxidant activity

The liver is the major organ responsible for metabolism, detoxification, and secretory functions in the body. The production of radical species, specifically oxygen and nitrogen radicals (ROS and RNS), has been proposed as an early event of drug-induced hepatotoxicity and as an indicator of hepatotoxic potential [85]. Presently, almost 1000 drugs, toxins, and herbs have been reported to cause liver injury [86]. It is in the liver that Phase I metabolism of drugs is realized. These

Table 3
Inhibitory activity of compounds **3d-g** against hCES1, hCES2, and porcine liver CES.

Compound	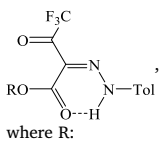 where R:	IC_{50} (μM) ± SEM			Selectivity Ratio		
		hCES1	hCES2	Porcine liver CES	hCES1/hCES2	hCES1/CES	hCES2/CES
3d	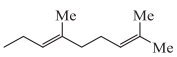	0.054 ± 0.005	0.00496 ± 0.00039	0.028 ± 0.002	11	1.9	0.18
3e		0.059 ± 0.005	0.00648 ± 0.00052	0.013 ± 0.001	9.2	4.5	0.50
3f	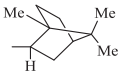	0.098 ± 0.008	2.10 ± 0.18	0.030 ± 0.003	0.05	3.3	70
3g	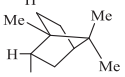	0.087 ± 0.007	0.132 ± 0.012	0.036 ± 0.003	0.66	2.4	3.7

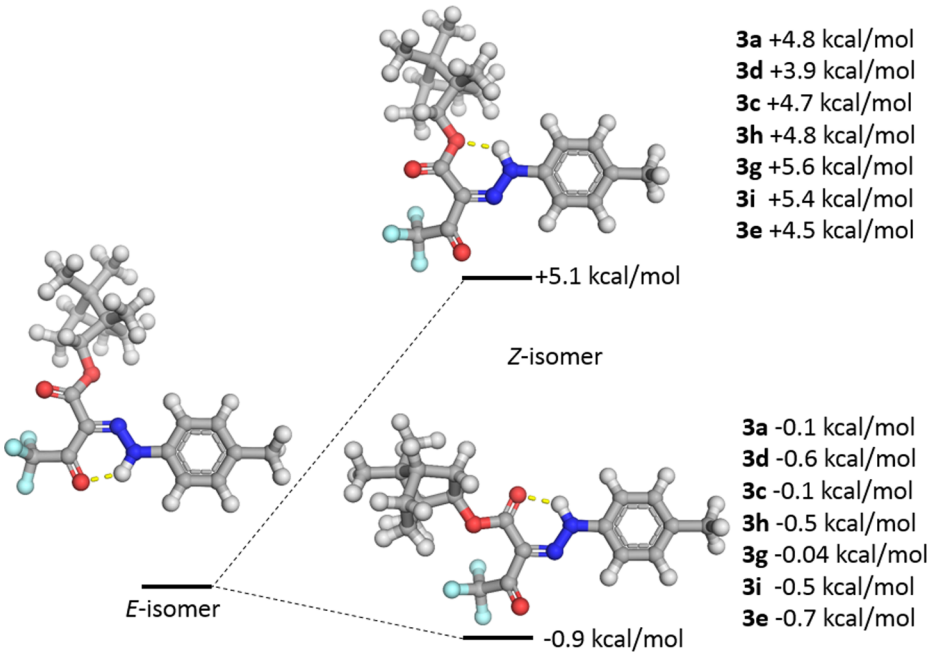

Fig. 4. QM energy minimization of the hydrazone tautomer **I** of compound **3f**, *E*- and *Z*-isomers. For the *Z*-isomer, two possible conformations with intramolecular hydrogen bonds (with ether and carbonyl oxygen atoms) are shown. For the other compounds, the energy differences of the two conformers of the *Z*-isomers relative to *E*-isomer energy level are listed.

biotransformations can involve oxidation reactions catalyzed by NADPH-dependent cytochrome P450 (CYP) enzymes, often resulting in the formation of the reactive radical species ROS and RNS. In addition, hydrolysis reactions catalyzed by CES enzymes can take place. These enzymes have a close intracellular localization in hepatocytes: CYP enzymes are localized in the microsomal fraction, and CES1 enzymes are distributed in both the microsomal and cytosolic fractions [34,35,87]. Moreover, it has been shown that the hepatoprotective effect of several exogenous compounds is closely associated with their antioxidant capacity [88,89]. Considering these connections, we assessed the antioxidant properties of the new CES inhibitors as additional attributes that could potentially contribute to beneficial effects such as hepatoprotection.

The antioxidant activity of the synthesized compounds **3a,c-i** was evaluated by means of the ABTS radical cation ($ABTS^{\bullet+}$) scavenging assay [40], using Trolox as the standard antioxidant. For the most active compounds, we also determined IC_{50} values (compound concentration required for 50% reduction of the ABTS radical).

As shown in Table 1, the $ABTS^{\bullet+}$-scavenging activity of all tested compounds **3a,c–i** was comparable to that of Trolox (TEAC range 0.86–1.1) and similar to that of the other known antioxidants, ascorbic acid and catechol. Thus, 3-oxo-2-tolylhydrazonylidene-4,4,4-trifluorobutanoates **3a,c–i** bearing higher and natural alcohol moieties were found to be potent antioxidants. Accordingly, we anticipate that the antiradical action of the developed selective inhibitors of CES enzymes is an additional useful feature that could protect the liver from damage induced by highly reactive metabolites formed during the P450-mediated biotransformation of drugs. Further research would be required to test this hypothesis.

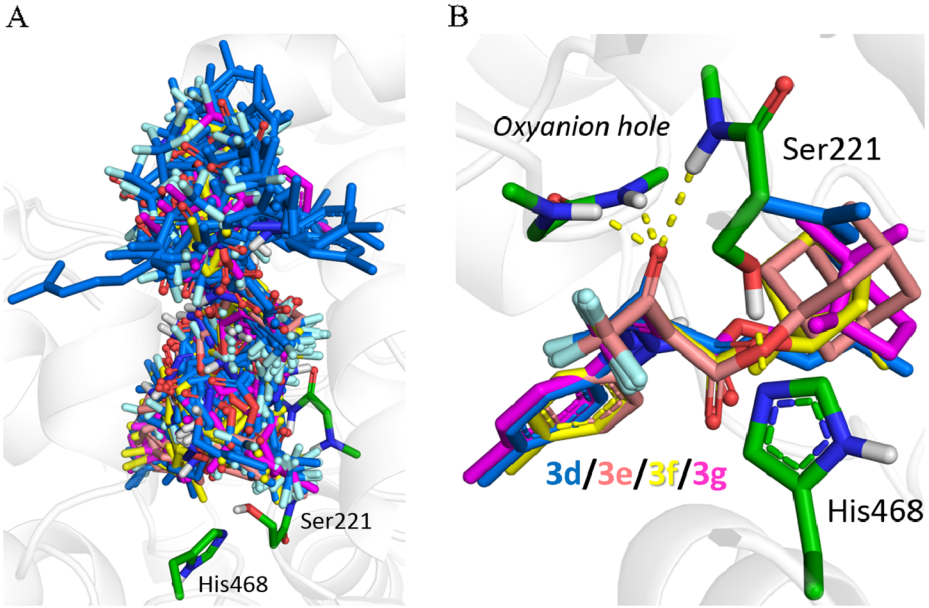

Fig. 5. Molecular docking poses of compounds in hCES1. (**A**) All docked poses spanning the entire gorge. (**B**) Poses in the catalytic active site equivalent to positions of substrates. Color key for carbon atoms in compounds: **3d** (blue), **3e** (salmon), **3f** (yellow) and **3g** (magenta).

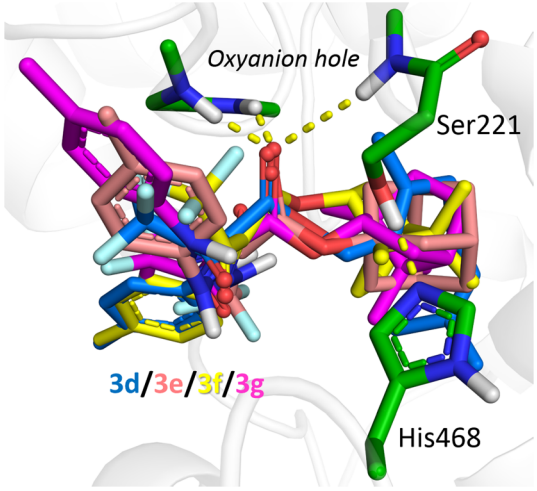

Fig. 6. Active site of the optimized homology model structure of porcine CES with binding poses of compounds inside the catalytic active site. The carbon atoms of compounds **3d,e,f,g** are colored as indicated, consistent with the color scheme in Fig. 5. Catalytic residues are numbered according to the human enzyme.

3.7. Acute toxicity studies

For all CES inhibitors, acute toxicity was determined on adult male CD-1 mice. For the tested compounds **3a,c-i**, 14-day survival was 100% for i.p. doses up to 300 mg/kg, indicating their favorable prospects as compounds with relatively low acute toxicity.

3.8. Predicted ADMET profiles of compounds *3a,c-i*

In order to assess the suitability of the potential lead compounds 3-oxo-2-tolylhydrazonylidene-4,4,4-trifluorobutanoates **3a,c-i** containing fragments of higher and natural alcohols for *in vivo* applications, we performed a preliminary computational estimation of some ADMET properties that may be relevant in the drug development context. In particular, human intestinal absorption (HIA) [55], blood-brain barrier permeability (LogBB) [56], and hERG-mediated cardiac toxicity risk (channel affinity pK_i and inhibitory activity pIC_{50}) [57] were estimated using predictive QSAR models based on accurate and representative training sets, fragmental descriptors, and artificial neural networks. The predicted properties of the compounds **3a,c-i** (Table 4) seem quite acceptable for early lead candidates, including excellent intestinal absorption, medium blood-brain barrier permeability, and low hERG liability risks. Moreover, the ADMET properties can be easily optimized at later stages of development. Thus, 3-oxo-2-tolylhydrazonylidene-4,4,4-trifluorobutanoates **3a,c-i** could potentially be used to modulate the pharmacokinetic behavior of ester-containing drugs.

Table 4
Predicted ADMET profiles of compounds **3a,c-i**.

Compound	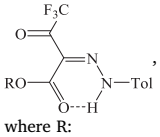 where R:	HIA	LogBB	hERG_ pK_i	hERG_ pIC_{50}
3a	n-C_6H_{13}	93.43	0.23	4.84	4.90
3c	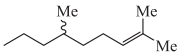	100.00	0.51	4.67	4.82
3d	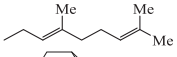	100.00	−0.18	4.50	4.93
3e	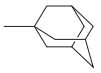	93.43	0.58	5.12	5.45
3f	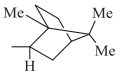	93.43	0.13	4.93	5.01
3g	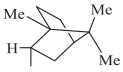	93.43	0.13	4.93	5.01
3h	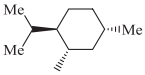	87.68	0.61	4.82	4.93
3i	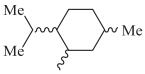	87.68	0.61	4.82	4.93

Note: HIA – human intestinal absorption [%], LogBB – blood-brain barrier permeability, hERG pK_i – hERG potassium channel affinity [–log(M)], hERG pIC_{50} – hERG potassium channel inhibitory activity [–log(M)].

4. Conclusions

In summary, a novel series of 3-oxo-2-tolylhydrazinylidene-4,4,4-trifluorobutanoates **3** bearing higher or natural alcohol moieties was synthesized via pre-transesterification of ethyl trifluoroacetylacetate with alcohols to isolate transesterificated oxoesters as lithium salts, which were then subjected to azo coupling with tolyldiazonium chloride. Their inhibitory activity against porcine liver CES, hCES1, hCES2, along with human erythrocyte AChE and equine serum BChE were investigated using enzyme kinetics and molecular docking. The results demonstrated that the compounds did not inhibit AChE and BChE and were effective and highly selective reversible mixed-type inhibitors of porcine liver CES.

Analysis of the X-ray crystallographic data together with IR and NMR spectra and QM calculations indicated that the *Z*-isomers were the most stable.

Molecular docking of the *Z*-isomers showed their binding in the catalytic active site, with carbonyl oxygen atoms in the oxyanion hole, suggesting the possibility of further covalent interactions, as well as non-specific binding outside of the active site. This makes the studied keto-esters interesting for further experimental kinetic and computational exploration (in particular, with QM/MM methods).

Some compounds proved to be highly active inhibitors of the main human isoenzymes hCES1 and hCES2. Namely, the esters of geraniol (**3d**) and adamantol (**3e**) were active in the nanomolar range and selective inhibitors of CES2. In contrast, esters of borneol (**3f**) and isoborneol (**3g**) were more selective for CES1.

Computational ADMET studies revealed that all compounds were predicted to have excellent intestinal absorption, medium blood-brain barrier permeability, and low hERG liability risks. In addition, all of the tested compounds possessed potentially useful radical-scavenging properties and low acute toxicity. Overall, the results indicate that members of a novel series of 3-oxo-2-tolylhydrazinylidene-4,4,4-trifluorobutanoates bearing higher or natural alcohol moieties have the potential to be good candidates as hCES1 or hCES2 inhibitors for biomedicinal applications.

Acknowledgements

The work was supported in part by the Russian State assignment No. AAAA-A19-119011790130-3 to IOS UB RAS (synthesis, X-ray analysis) and Russian State assignment No. 0090-2017-0019 to IPAC RAS (biochemical study). Analytical studies were carried out using equipment of the Center for Joint Use “Spectroscopy and Analysis of Organic Compounds” at the Postovsky Institute of Organic Synthesis of the Russian Academy of Sciences (Ural Branch). Computer modeling was carried out using equipment from the shared research facilities of the HPC computing resources at Lomonosov Moscow State University [52] and the KazD JSCC RAS – branch of SRISA. We are also grateful to the Center of the Collective-Access Equipment of the Institute of Physiologically Active Compounds, Russian Academy of Sciences for

use of equipment. Support for RJR's contributions were provided by the University of Michigan. The funding sources had no role in the study design; collection, analysis and interpretation of data; writing of the manuscript; or the decision to submit the article for publication. The authors thank Dr. O.P. Krasnykh (Perm National Research Polytechnic University, Russia) for determination of acute toxicity.

Declaration of Competing Interest

The authors have declared no conflict of interest.

Appendix A. Supplementary material

Supplementary data to this article can be found online at https://doi.org/10.1016/j.bioorg.2019.103097.

References

[1] M. Hosokawa, Structure and catalytic properties of carboxylesterase isozymes involved in metabolic activation of prodrugs, Molecules 13 (2) (2008) 412–431, https://doi.org/10.3390/molecules13020412.
[2] S.C. Laizure, V. Herring, Z. Hu, K. Witbrodt, R.B. Parker, The role of human carboxylesterases in drug metabolism: have we overlooked their importance? Pharmacotherapy 33 (2) (2013) 210–222, https://doi.org/10.1002/phar.1194.
[3] J.L. Staudinger, C. Xu, Y.J. Cui, C.D. Klaassen, Nuclear receptor-mediated regulation of carboxylesterase expression and activity, Expert Opin. Drug Metab. Toxicol. 6 (3) (2010) 261–271, https://doi.org/10.1517/17425250903483215.
[4] S.P. Sanghani, P.C. Sanghani, M.A. Schiel, W.F. Bosron, Human carboxylesterases: an update on CES1, CES2 and CES3, Protein Peptide Lett. 16 (10) (2009) 1207–1214, https://doi.org/10.2174/092986609789071324.
[5] T. Imai, Human carboxylesterase isozymes: catalytic properties and rational drug design, Drug Metab. Pharmacokinet. 21 (3) (2006) 173–185, https://doi.org/10.2133/dmpk.21.173.
[6] J. Lian, R. Nelson, R. Lehner, Carboxylesterases in lipid metabolism: from mouse to human, Protein Cell 9 (2) (2018) 178–195, https://doi.org/10.1007/s13238-017-0437-z.
[7] S. Mukherjee, M. Choi, J.W. Yun, Novel regulatory roles of carboxylesterase 3 in lipid metabolism and browning in 3T3-L1 white adipocytes, Appl. Physiol. Nutr. Metab. (2019), https://doi.org/10.1139/apnm-2018-0814.
[8] L. Yang, X. Li, H. Tang, Z. Gao, K. Zhang, K. Sun, A unique role of carboxylesterase 3 (Ces3) in beta-adrenergic signaling-stimulated thermogenesis, Diabetes 68 (6) (2019) 1178–1196, https://doi.org/10.2337/db18-1210.
[9] M.J. Hatfield, L. Tsurkan, M. Garrett, T.M. Shaver, J.L. Hyatt, C.C. Edwards, L.D. Hicks, P.M. Potter, Organ-specific carboxylesterase profiling identifies the small intestine and kidney as major contributors of activation of the anticancer prodrug CPT-11, Biochem. Pharmacol. 81 (1) (2011) 24–31, https://doi.org/10.1016/j.bcp.2010.09.001.
[10] L. Di, The impact of carboxylesterases in drug metabolism and pharmacokinetics, Curr. Drug Metab. 20 (2) (2019) 91–102, https://doi.org/10.2174/1389200219666180821094502.
[11] L.W. Zou, Q. Jin, D.D. Wang, Q.K. Qian, D.C. Hao, G.B. Ge, L. Yang, Carboxylesterase inhibitors: an update, Curr. Med. Chem. 25 (14) (2018) 1627–1649, https://doi.org/10.2174/0929867325666171204155558.
[12] K.J. Yoon, J.L. Hyatt, C.L. Morton, R.E. Lee, P.M. Potter, M.K. Danks, Characterization of inhibitors of specific carboxylesterases: development of carboxylesterase inhibitors for translational application, Mol. Cancer Ther. 3 (8) (2004) 903–909.
[13] M.J. Hatfield, P.M. Potter, Carboxylesterase inhibitors, Expert Opin. Ther. Pat. 21 (8) (2011) 1159–1171, https://doi.org/10.1517/13543776.2011.586339.
[14] P. Potter, R. Wadkins, Carboxylesterases – detoxifying enzymes and targets for drug therapy, Curr. Med. Chem. 13 (9) (2006) 1045–1054, https://doi.org/10.2174/092986706776360969.
[15] G.R. Mukhamadieva, N.P. Boltneva, T.G. Galenko, V.B. Sokolov, T.A. Epishina, G.F. Makhaeva, Synthesis and biological activity of O-carbamoylated 1,1,1,3,3,3-hexafluoroisopropanols as new specific inhibitors of carboxylesterase, Pharm. Chem. J. 46 (8) (2012) 461–464, https://doi.org/10.1007/s11094-012-0825-x.
[16] E. Dominguez, A. Galmozzi, J.W. Chang, K.L. Hsu, J. Pawlak, W. Li, C. Godio, J. Thomas, D. Partida, S. Niessen, P.E. O'Brien, A.P. Russell, M.J. Watt, D.K. Nomura, B.F. Cravatt, E. Saez, Integrated phenotypic and activity-based profiling links Ces3 to obesity and diabetes, Nat. Chem. Biol. 10 (2) (2014) 113–121, https://doi.org/10.1038/nchembio.1429.
[17] Y.J. Liu, S.Y. Li, J. Hou, Y.F. Liu, D.D. Wang, Y.S. Jiang, G.B. Ge, X.M. Liang, L. Yang, Identification and characterization of naturally occurring inhibitors against human carboxylesterase 2 in White Mulberry Root-bark, Fitoterapia 115 (2016) 57–63, https://doi.org/10.1016/j.fitote.2016.09.022.
[18] D.D. Wang, L.W. Zou, Q. Jin, J. Hou, G.B. Ge, L. Yang, Recent progress in the discovery of natural inhibitors against human carboxylesterases, Fitoterapia 117 (2017) 84–95, https://doi.org/10.1016/j.fitote.2017.01.010.
[19] A. De Palma, R. Rossi, M. Carai, C. Cabras, G. Colombo, L. Arnoldi, N. Fuzzati, A. Riva, P. Morazzoni, P.L. Mauri, Pharmaceutical and biomedical analysis of terpene constituents in Salvia miltiorrhiza, Curr. Pharm. Anal. 4 (4) (2008) 249–257, https://doi.org/10.2174/157341208786306207.
[20] M.J. Hatfield, L.G. Tsurkan, J.L. Hyatt, C.C. Edwards, A. Lemoff, C. Jeffries, B. Yan, P.M. Potter, Modulation of esterified drug metabolism by tanshinones from Salvia miltiorrhiza ("Danshen"), J. Nat. Prod. 76 (1) (2013) 36–44, https://doi.org/10.1021/np300628a.
[21] M.J. Hatfield, J. Chen, E.M. Fratt, L. Chi, J.C. Bollinger, R.J. Binder, J. Bowling, J.L. Hyatt, J. Scarborough, C. Jeffries, P.M. Potter, Selective inhibitors of human liver carboxylesterase based on a beta-lapachone scaffold: novel reagents for reaction profiling, J. Med. Chem. 60 (4) (2017) 1568–1579, https://doi.org/10.1021/acs.jmedchem.6b01849.
[22] L. Wen, Y. Jiang, J. Yang, Y. Zhao, M. Tian, B. Yang, Structure, bioactivity, and synthesis of methylated flavonoids, Ann. NY Acad. Sci. 1398 (1) (2017) 120–129, https://doi.org/10.1111/nyas.13350.
[23] C. Santos-Buelga, A.S. Feliciano, Flavonoids: from structure to health issues, Molecules 22 (3) (2017), https://doi.org/10.3390/molecules22030477.
[24] D.X. Sun, G.B. Ge, P.P. Dong, Y.F. Cao, Z.W. Fu, R.X. Ran, X. Wu, Y.Y. Zhang, H.M. Hua, Z. Zhao, Z.Z. Fang, Inhibition behavior of fructus psoraleae's ingredients towards human carboxylesterase 1 (hCES1), Xenobiotica 46 (6) (2016) 503–510, https://doi.org/10.3109/00498254.2015.1091521.
[25] Y.G. Li, J. Hou, S.Y. Li, X. Lv, J. Ning, P. Wang, Z.M. Liu, G.B. Ge, J.Y. Ren, L. Yang, Fructus psoraleae contains natural compounds with potent inhibitory effects towards human carboxylesterase 2, Fitoterapia 101 (2015) 99–106, https://doi.org/10.1016/j.fitote.2015.01.004.
[26] M. Zhou, R.H. Zhang, M. Wang, G.B. Xu, S.G. Liao, Prodrugs of triterpenoids and their derivatives, Eur. J. Med. Chem. 131 (2017) 222–236, https://doi.org/10.1016/j.ejmech.2017.03.005.
[27] I. Zebiri, M. Haddad, L. Duca, M. Sauvain, L. Paloque, B. Cabanillas, E. Rengifo, J.B. Behr, L. Voutquenne-Nazabadioko, Biological activities of triterpenoids from Poraqueiba sericea stems, Nat. Prod. Res. 31 (11) (2017) 1333–1338, https://doi.org/10.1080/14786419.2016.1241998.
[28] L.W. Zou, T.Y. Dou, P. Wang, W. Lei, Z.M. Weng, J. Hou, D.D. Wang, Y.M. Fan, W.D. Zhang, G.B. Ge, L. Yang, Structure-Activity Relationships of pentacyclic triterpenoids as potent and selective inhibitors against human carboxylesterase 1, Front. Pharmacol. 8 (2017) 435, https://doi.org/10.3389/fphar.2017.00435.
[29] Y.V. Burgart, G.F. Makhaeva, E.V. Shchegol'kov, O.G. Khudina, N.P. Boltneva, O.G. Serebryakova, S.V. Lushchekina, V.I. Saloutin, S.O. Bachurin, O.N. Chupakhin, Selective carboxylesterase inhibitors representing alkyl-2-arylhydrazinylidene-3-oxo-polyfluoroalkylpropionates, methods for production and use thereof, Patent RU 2574291C1 (2014).
[30] N.P. Boltneva, G.F. Makhaeva, N.V. Kovaleva, S.V. Lushchekina, Y.V. Burgart, E.V. Shchegol'kov, V.I. Saloutin, O.N. Chupakhin, Alkyl 2-arylhydrazinylidene-3-oxo-3-polyfluoroalkylpropionates as new effective and selective inhibitors of carboxylesterase, Dokl. Biochem. Biophys. 465 (2015) 381–385, https://doi.org/10.1134/S1607672915060101.
[31] N.P. Boltneva, G.F. Makhaeva, E.V. Shchegol'kov, Y.V. Burgart, V.I. Saloutin, Selective carboxylesterase inhibitors for improving efficacy, safety and rational use of ester-containing drugs, Biomed. Chem. Res. Meth. 1 (3) (2018) e00026, https://doi.org/10.18097/bmcrm00026.
[32] G.F. Makhaeva, E.V. Rudakova, N.V. Kovaleva, S.V. Lushchekina, N.P. Boltneva, V.V. Proshin, E.V. Shchegol'kov, Y.V. Burgart, V.I. Saloutin, Cholinesterase and carboxylesterase inhibitors as pharmacological agents, Russ. Chem. Bull. 68 (5) (2019) 967–984.
[33] E.V. Shchegol'kov, G.F. Makhaeva, N.P. Boltneva, S.V. Lushchekina, O.G. Serebryakova, E.V. Rudakova, N.V. Kovaleva, Y.V. Burgart, V.I. Saloutin, O.N. Chupakhin, S.O. Bachurin, R.J. Richardson, Synthesis, molecular docking, and biological activity of polyfluoroalkyl dihydroazolo[5,1-c][1,2,4]triazines as selective carboxylesterase inhibitors, Bioorg. Med. Chem. 25 (15) (2017) 3997–4007, https://doi.org/10.1016/j.bmc.2017.05.045.
[34] A. Parkinson, B.W. Ogilvie, D.B. Buckley, F. Kazmi, M. Czerwinski, O. Parkinson, Biotransformation of xenobiotics, in: C.D. Klaassen, J.B. Watkins, C.D. Klaassen, J.B. Watkins (Eds.), Casarett & Doull's Essentials of Toxicology, The McGraw-Hill Companies, Inc, New York, 2015, pp. 79–107.
[35] L. Hedges, S. Brown, A.K. MacLeod, A. Vardy, E. Doyle, G. Song, M. Moreau, M. Yoon, T.G. Osimitz, B.G. Lake, Metabolism of deltamethrin and cis- and trans-permethrin by human expressed cytochrome P450 and carboxylesterase enzymes, Xenobiotica 49 (5) (2019) 521–527, https://doi.org/10.1080/00498254.2018.14742834.
[36] G. Sheldrick, Shelx-84 – a program system for crystal-structure solution and refinement, Acta Crystallogr. A 40 (1984), https://doi.org/10.1107/S010876738408702x C440-C440.
[37] O.G. Khudina, E.V. Shchegol'kov, Y.V. Burgart, M.I. Kodess, O.N. Kazheva, A.N. Chekhlov, G.V. Shilov, O.A. Dyachenko, V.I. Saloutin, O.N. Chupakhin, Synthesis and the reactions of trifluoromethylated 1,2,3-triketones 2-(het)arylhydrazones and 4,7-dihydroazolo[5,1-c]triazines, J. Fluor. Chem. 126 (8) (2005) 1230–1238, https://doi.org/10.1016/j.jfluchem.2005.06.001.
[38] G.L. Ellman, K.D. Courtney, V. Andres, R.M. Featherstone, A new and rapid colorimetric determination of acetylcholinesterase activity, Biochem. Pharmacol. 7 (2) (1961) 88–95, https://doi.org/10.1016/0006-2952(61)90145-9.
[39] S.H. Sterri, B.A. Johnsen, F. Fonnum, A radiochemical assay method for carboxylesterase, and comparison of enzyme activity towards the substrates methyl [1-14C] butyrate and 4-nitrophenyl butyrate, Biochem. Pharmacol. 34 (15) (1985) 2779–2785, https://doi.org/10.1016/0006-2952(85)90579-9.
[40] R. Re, N. Pellegrini, A. Proteggente, A. Pannala, M. Yang, C. Rice-Evans, Antioxidant activity applying an improved ABTS radical cation decolorization assay, Free Radic. Biol. Med. 26 (9–10) (1999) 1231–1237, https://doi.org/10.1016/s0891-5849(98)00315-3.
[41] Federal Law of 12.04.2010. №61-FZ RF On Circulation of Medicines.
[42] A.N. Mironov, Guidelines for pre-clinical study of medicinal products (in Russian), Grif&Ko, Moscow, 2012.
[43] Paris: OECD 1996 OECD Guideline 423: Acute oral toxicity.
[44] M.W. Schmidt, K.K. Baldridge, J.A. Boatz, S.T. Elbert, M.S. Gordon, J.H. Jensen, S. Koseki, N. Matsunaga, K.A. Nguyen, S. Su, T.L. Windus, M. Dupuis,

J.A. Montgomery, General atomic and molecular electronic structure system, J. Comput. Chem. 14 (11) (1993) 1347–1363, https://doi.org/10.1002/jcc.540141112.
[45] R.S. Mulliken, Electronic population analysis on LCAO–MO molecular wave functions. I, J. Chem. Phys. 23 (10) (1955) 1833–1840, https://doi.org/10.1063/1.1740588.
[46] S. Bencharit, C.C. Edwards, C.L. Morton, E.L. Howard-Williams, P. Kuhn, P.M. Potter, M.R. Redinbo, Multisite promiscuity in the processing of endogenous substrates by human carboxylesterase 1, J. Mol. Biol. 363 (1) (2006) 201–214, https://doi.org/10.1016/j.jmb.2006.08.025.
[47] G.F. Makhaeva, N.P. Boltneva, S.V. Lushchekina, O.G. Serebryakova, T.S. Stupina, A.A. Terentiev, I.V. Serkov, A.N. Proshin, S.O. Bachurin, R.J. Richardson, Synthesis, molecular docking and biological evaluation of N, N-disubstituted 2-aminothiazolines as a new class of butyrylcholinesterase and carboxylesterase inhibitors, Bioorg. Med. Chem. 24 (5) (2016) 1050–1062, https://doi.org/10.1016/j.bmc.2016.01.031.
[48] B. Webb, A. Sali, Comparative protein structure modeling using MODELLER, Curr. Protoc. Bioinformatics 54 (2016) 5.6.1-5.6.37. 10.1002/cpbi.3.
[49] V.B. Chen, W.B. Arendall 3rd, J.J. Headd, D.A. Keedy, R.M. Immormino, G.J. Kapral, L.W. Murray, J.S. Richardson, D.C. Richardson, MolProbity: all-atom structure validation for macromolecular crystallography, Acta Crystallogr. D 66 (Pt 1) (2010) 12–21, https://doi.org/10.1107/S0907444909042073.
[50] J.C. Phillips, R. Braun, W. Wang, J. Gumbart, E. Tajkhorshid, E. Villa, C. Chipot, R.D. Skeel, L. Kale, K. Schulten, Scalable molecular dynamics with NAMD, J. Comput. Chem. 26 (16) (2005) 1781–1802, https://doi.org/10.1002/jcc.20289.
[51] J. Huang, A.D. MacKerell Jr., CHARMM36 all-atom additive protein force field: validation based on comparison to NMR data, J. Comput. Chem. 34 (25) (2013) 2135–2145, https://doi.org/10.1002/jcc.23354.
[52] V. Sadovnichy, A. Tikhonravov, V. Voevodin, V. Opanasenko, "Lomonosov": supercomputing at Moscow State University, in: J.S. Vetter (Ed.), Contemporary High Performance Computing: From Petascale toward Exascale, CRC Press, Boca Raton, USA, 2013, pp. 283–307.
[53] G.M. Morris, D.S. Goodsell, R.S. Halliday, R. Huey, W.E. Hart, R.K. Belew, A.J. Olson, Automated docking using a Lamarckian genetic algorithm and an empirical binding free energy function, J. Comput. Chem. 19 (14) (1998) 1639–1662, https://doi.org/10.1002/(sici)1096-987x(19981115)19:14<1639::aid-jcc10>3.0.co;2-b.
[54] G.M. Morris, R. Huey, W. Lindstrom, M.F. Sanner, R.K. Belew, D.S. Goodsell, A.J. Olson, AutoDock4 and AutoDockTools4: automated docking with selective receptor flexibility, J. Comput. Chem. 30 (16) (2009) 2785–2791, https://doi.org/10.1002/jcc.21256.
[55] E.V. Radchenko, A.S. Dyabina, V.A. Palyulin, N.S. Zefirov, Prediction of human intestinal absorption of drug compounds, Russ. Chem. Bull. 65 (2) (2016) 576–580, https://doi.org/10.1007/s11172-016-1340-0.
[56] A.S. Dyabina, E.V. Radchenko, V.A. Palyulin, N.S. Zefirov, Prediction of blood-brain barrier permeability of organic compounds, Dokl Biochem. Biophys. 470 (1) (2016) 371–374, https://doi.org/10.1134/S1607672916050173.
[57] E.V. Radchenko, Y.A. Rulev, A.Y. Safanyaev, V.A. Palyulin, N.S. Zefirov, Computer-aided estimation of the hERG-mediated cardiotoxicity risk of potential drug components, Dokl. Biochem. Biophys. 473 (1) (2017) 128–131, https://doi.org/10.1134/S1607672917020107.
[58] ADMET Prediction Service. http://qsar.chem.msu.ru/admet/ (Accessed 01 Jul 2018).
[59] R.J. Clemens, Diketene, Chem. Rev. 86 (2) (1986) 241–318, https://doi.org/10.1021/cr00072a001.
[60] T. Yamamoto, S. Niwa, S. Ohno, T. Onishi, H. Matsueda, H. Koganei, H. Uneyama, S. Fujita, T. Takeda, M. Kito, Y. Ono, Y. Saitou, A. Takahara, S. Iwata, M. Shoji, Structure-activity relationship study of 1,4-dihydropyridine derivatives blocking N-type calcium channels, Bioorg. Med. Chem. Lett. 16 (4) (2006) 798–802, https://doi.org/10.1016/j.bmcl.2005.11.021.
[61] G. Krishnaiah, K.C. Rajanna, K.R. Reddy, M.S. Kumar, P. Srinivas, Y.R. Rao, Cesium carbonate as efficient catalyst for chemoselective transesterification of β-ketoesters under conventional and unconventional conditions, Res. Chem. Interm. 41 (5) (2013) 2739–2751, https://doi.org/10.1007/s11164-013-1383-x.
[62] G. Krishnaiah, B. Sandeep, D. Kondhare, K.C. Rajanna, J. Narendar Reddy, Y. Rajeshwar Rao, P.K. Zhubaidha, Manganese(II) salts as efficient catalysts for chemo selective transesterification of β-keto esters under non-conventional conditions, Tetrahedron Lett. 54 (7) (2013) 703–706, https://doi.org/10.1016/j.tetlet.2012.12.030.
[63] B. Clapham, S.-H. Lee, G. Koch, J. Zimmermann, K.D. Janda, The preparation of polymer bound β-ketoesters and their conversion into an array of oxazoles, Tetrahedron Lett. 43 (31) (2002) 5407–5410, https://doi.org/10.1016/s0040-4039(02)01076-6.
[64] T. Masuyama, M. Shimada, Method for producing ester compound and transesterification catalyst, Japan, Patent #2010150190 (2010).
[65] M.E. Meyer, E.M. Ferreira, B.M. Stoltz, 2-Diazoacetoacetic acid, an efficient and convenient reagent for the synthesis of alpha-diazo-beta-ketoesters, Chem. Commun. (Camb) 12 (2006) 1316–1318, https://doi.org/10.1039/b517719g.
[66] N. Hiromitsu, K. Reiko, N. Kazuo, S. Mitsuo, Radiation-sensitive resin composition, polymer, and compound, Patent #2012033138 (2012).
[67] M. Lakshmi Kantam, V. Neeraja, B. Bharathi, C. Venkat Reddy, Transesterification of β -keto esters catalysed by transition metal complexes in a novel heterogeneous way, Catal. Lett. 62 (1) (1999) 67–69, https://doi.org/10.1023/a: 1019074300785.
[68] G.B. Dharma Rao, M.P. Kaushik, Efficient trans-acetoacylation mediated by ytterbium(III) triflate as a catalyst under solvent-free condition, Tetrahedron Lett. 52 (39) (2011) 5104–5106, https://doi.org/10.1016/j.tetlet.2011.07.108.
[69] I. Shimizu, H. Ishii, A. Tasaka, Facile synthesis of trifluoromethyl ketones by palladium-catalyzed Carroll type reaction, Chem. Lett. 18 (7) (1989) 1127–1128, https://doi.org/10.1246/cl.1989.1127.
[70] B. Madje, P. Patil, S. Shindalkar, S. Benjamin, M. Shingare, M. Dongare, Facile transesterification of β-ketoesters under solvent-free condition using borate zirconia solid acid catalyst, Catal. Comm. 5 (7) (2004) 353–357, https://doi.org/10.1016/j.catcom.2004.04.004.
[71] V.I. Saloutin, P.N. Kondrat'ev, Z.E. Skryabina, Transesterification of copper(II) β-ketoesterates and acylpyruvates with borneol, Russ. Chem. Bull. 42 (5) (1993) 858–860, https://doi.org/10.1007/bf00698945.
[72] F.C. da Silva, V.F. Ferreira, R.S. Rianelli, W.C. Perreira, Natural clays as efficient catalyst for transesterification of β-keto esters with carbohydrate derivatives, Tetrahedron Lett. 43 (7) (2002) 1165–1168, https://doi.org/10.1016/s0040-4039(01)02388-7.
[73] H.P. Beck, S.K. Booker, H. Bregman, V.J. Cee, N. Chakka, T.D. Cushing, O.E., B.M. Fox, S. Geuns-Meyer, X. Hao, K. Hibiya, J. Hirata, Z. Hua, J. Human, S. Kakuda, P. Lopez, R. Nakajima, K. Okada, S.H. Olson, H. Oono, L.D. Pennington, K. Sasaki, K. Shimada, Y. Shin, R.D. White, R.P. Wurz, S. Yi, X.M. Zheng, Pyrazole amide derivative, Patent #2015129926 (2015).
[74] G.B. Dharma Rao, B.N. Acharya, M.P. Kaushik, An efficient synthesis of β-ketoesters via transesterification and its application in Biginelli reaction under solvent-free, catalyst-free conditions, Tetrahedron Lett. 54 (48) (2013) 6644–6647, https://doi.org/10.1016/j.tetlet.2013.09.130.
[75] L.I. Koval, V.I. Dzyuba, O.L. Ilnitska, V.I. Pekhnyo, Efficient transesterification of ethyl acetoacetate with higher alcohols without catalysts, Tetrahedron Lett. 49 (10) (2008) 1645–1647, https://doi.org/10.1016/j.tetlet.2008.01.018.
[76] O.G. Khudina, Y.V. Burgart, E.V. Shchegol'kov, V.I. Saloutin, O.N. Kazheva, A.N. Chekhlov, O.A. D'yachenko, Steric structure of alkyl 2-aryl(hetaryl)hydrazono-3-fluoroalkyl-3-oxopropionates, Russ. J. Org. Chem. 45 (6) (2009) 801–809, https://doi.org/10.1134/s1070428009060013.
[77] G.F. Makhaeva, E.V. Radchenko, V.A. Palyulin, E.V. Rudakova, A.Y. Aksinenko, V.B. Sokolov, N.S. Zefirov, R.J. Richardson, Organophosphorus compound esterase profiles as predictors of therapeutic and toxic effects, Chem. Biol. Interact 203 (1) (2013) 231–237, https://doi.org/10.1016/j.cbi.2012.10.012.
[78] G.F. Makhaeva, E.V. Rudakova, O.G. Serebryakova, A.Y. Aksinenko, S.V. Lushchekina, S.O. Bachurin, R.J. Richardson, Esterase profiles of organophosphorus compounds in vitro predict their behavior in vivo, Chem. Biol. Interact 259 (Pt B) (2016) 332–342, https://doi.org/10.1016/j.cbi.2016.05.002.
[79] M. Harel, D.M. Quinn, H.K. Nair, I. Silman, J.L. Sussman, The X-ray structure of a transition state analog complex reveals the molecular origins of the catalytic power and substrate specificity of acetylcholinesterase, J. Am. Chem. Soc. 118 (10) (1996) 2340–2346, https://doi.org/10.1021/ja952232h.
[80] A.V. Nemukhin, S.V. Lushchekina, A.V. Bochenkova, A.A. Golubeva, S.D. Varfolomeev, Characterization of a complete cycle of acetylcholinesterase catalysis by ab initio QM/MM modeling, J. Mol. Model 14 (5) (2008) 409–416, https://doi.org/10.1007/s00894-008-0287-y.
[81] T. Bohnuud, L. Luo, S.J. Wodak, A.M. Bonvin, Z. Weng, S. Vajda, O. Schueler-Furman, D. Kozakov, A benchmark testing ground for integrating homology modeling and protein docking, Proteins 85 (1) (2017) 10–16, https://doi.org/10.1002/prot.25063.
[82] A. Bordogna, A. Pandini, L. Bonati, Predicting the accuracy of protein-ligand docking on homology models, J. Comput. Chem. 32 (1) (2011) 81–98, https://doi.org/10.1002/jcc.21601.
[83] J.A. Doering, S. Lee, K. Kristiansen, L. Evenseth, M.G. Barron, I. Sylte, C.A. LaLone, In silico site-directed mutagenesis informs species-specific predictions of chemical susceptibility derived from the Sequence Alignment to Predict Across Species Susceptibility (SeqAPASS) tool, Toxicol. Sci. 166 (1) (2018) 131–145, https://doi.org/10.1093/toxsci/kfy186.
[84] T.L. Gonzalez, J.M. Rae, J.A. Colacino, R.J. Richardson, Homology models of mouse and rat estrogen receptor-alpha ligand-binding domain created by in silico mutagenesis of a human template: molecular docking with 17β-estradiol, diethylstilbestrol, and paraben analogs, Comput. Toxicol. 10 (2019) 1–16, https://doi.org/10.1016/j.comtox.2018.11.003.
[85] L.A. Videla, Oxidative stress signaling underlying liver disease and hepatoprotective mechanisms, World J. Hepatol. 1 (1) (2009) 72–78, https://doi.org/10.4254/wjh.v1.i1.72.
[86] F.P. Busardò, G.A., Editorial – Drug-induced hepatotoxicity, Eur. Rev. Med. Pharmacol. Sci. 21 (1 Suppl) (2017) 135–137.
[87] S. Li, H.Y. Tan, N. Wang, Z.J. Zhang, L. Lao, C.W. Wong, Y. Feng, The role of oxidative stress and antioxidants in liver diseases, Int. J. Mol. Sci. 16 (11) (2015) 26087–26124, https://doi.org/10.3390/ijms161125942.
[88] G.A. de la Riva, F.J. Lopez Mendoza, G. Aguero-Chapin, Known hepatoprotectors act as antioxidants and immune stimulators in stressed mice: perspectives in animal health care, Curr. Pharm. Des. 24 (40) (2018) 4825–4837, https://doi.org/10.2174/1381612825666190116151628.
[89] A.K. Singal, S.C. Jampana, S.A. Weinman, Antioxidants as therapeutic agents for liver disease, Liver Int. 31 (10) (2011) 1432–1448, https://doi.org/10.1111/j.1478-3231.2011.02604.x.